Petroleum evolution within the Tarim Basin, NW China: Insights from organic geochemistry, fluid inclusions, and Re-Os geochronology of the Halahatang Oilfield

Xiang Ge[1,2], Chuanbo Shen[1*], David Selby[2,5], Martin Feely[3], Guangyou Zhu[4]

[1]Key Laboratory of Tectonics and Petroleum Resources (China University of Geosciences), Ministry of Education, Wuhan, 430074, China

[2]Department of Earth Sciences, Durham University, Durham, DH1 3LE, UK

[3]Earth and Ocean Sciences, School of Natural Sciences, National University of Ireland, Galway, Ireland

[4]Research Institute of Petroleum Exploration and Development, PetroChina, Beijing 100083, China

[5]State Key Laboratory of Geological Processes and Mineral Resources, School of Earth Resources, China University of Geosciences, Wuhan, 430074, China

***Corresponding author E-mail: cugshen@126.com**

Acknowledgements

This work was supported by the National Natural Science Foundation of China (No. 41802168, 41672140, 41372140), the PetroChina Innovation Foundation (No. 2016D-5007-0103), the Program of Introducing Talents of Discipline to Universities (No. B14031), the Outstanding Youth Funding of Natural Science Foundation of Hubei Province (No. 2016CFA055), and the Fundamental Research Fund for the Central Universities, China University of Geosciences (Wuhan, No. CUG180617, CUGCJ1820, CUGCJ1712), and Open Topic Fund from Key Laboratory of Tectonics and Petroleum Resources of Ministry of Education (TPR-2018-11). We thank Dr. Emmanuel Laverret of CV Associés Engineering, France for the fluid inclusion analysis and PVTx modelling.

DS acknowledges the Total Endowment Fund and the Dida Scholarship from CUG Wuhan. Xiang Ge was supported by a postgraduate award from the China Scholarship Council (CSC). We acknowledge the analytical support of Antonia Hofmann, Geoff Nowell and Chris Ottley. Lastly, we thank Barry J. Katz, Ling Gao and two anonymous reviewers for their constructive reviews which helped improve the paper.

Abstract

The newly discovered Halahatang oilfield in the northern Tarim Basin has a potential resource of > 70 Bbbls of oil. Oil organic geochemical data from the Halahatang oilfield indicate that the oils are of moderate maturity, biodegraded, and represent one oil family, derived from the same Paleozoic marine source. Modeling of coeval aqueous and hydrocarbon-bearing inclusion data provide fluid trapping temperatures and pressures of 100 to 110 ºC and ~39 to 59 MPa, respectively. The fluid inclusion data coupled with the previous basin model studies, suggests a single prolonged oil migration event during the Permian. Rhenium-Osmium (Re-Os) isotope data oil yield an Early Permian Re-Os age of 285 ± 48 Ma. The age agrees with the timing of maturation of the Paleozoic source via burial history modelling but is slightly older (~5 - 55 myr) than the oil migration/accumulation timing implied by the basin modelling coupled with fluid inclusion analysis and the published reservoir illite K-Ar dates. Thus, the oil Re-Os date suggests that oil generation in the Halahatang Depression of the Tarim Basin occurred during the Early Permian, rather than the Silurian as previously proposed, with subsequent oil migration/accumulation occurring during the Mid-Late Permian as recorded by basin modelling, coupled with fluid inclusion analysis and illite K-Ar dating. In addition to promoting petroleum exploration in the Tarim Basin, this study that combines crude oil Re-Os isotope dating and traditional analytical methods (organic geochemistry/fluid inclusion analysis) to constrain petroleum evolution is applicable to hydrocarbon systems worldwide.

Keywords

Petroleum evolution; Re-Os geochronology; Organic geochemistry; Fluid inclusions; Halahatang oilfield; Tarim Baisn

1 Introduction

The accurate key timing of petroleum evolution (e.g., oil generation, migration / accumulation) is vital to understand the evolution of a petroleum system (Liu et al., 2013; Qiu et al., 2011), and is crucial for hydrocarbon exploration in a target region (Roberts et al., 2004). Although thousands of oilfields are known worldwide, understanding how to precisely constrain the key events of a petroleum system remains challenging (Liu et al., 2013; Mark et al., 2010; Roberts et al., 2004). Aimed at solving these problems, the oilfield in Tarim Basin, northwest China was selected as an example in this study. The Tarim basin is bordered by the Tian Shan, West Kunlun and A'erjin orogenic belts to the north, southwest, and southeast, respectively (Lin et al., 2015; Zhang et al., 2007a) (Fig. 1B). The basin encompasses an area of 560,000 km^2 (~216,217 mi^2) and contains up to ~14 km (~8.7 mi) of sedimentary strata. It has had a complex tectonic evolution (e.g., Caledonian, Hercynian, Indosinian-Yanshan and Himalayan orogenies). The basin contains significant petroleum potential (more than 70 billion barrels oil (Bbbls) and 250 trillion cubic feet (Tcf) of gas) (Lin et al., 2015; Xiao and Tang, 2003; Xu et al., 2004). The Tarim Basin is the largest known onshore petroliferous basin in China, with only an estimated 10 percent of the total potential reserves presently discovered (Li, 2009; Xu et al., 2004). Although the Tarim Basin is considered to contain the most important future oil and gas resources in China (Li, 2009), the multiple tectonic events that the basin

records have led to a complex hydrocarbon evolution, which has hampered oil and gas exploration (Li, 2009; Lin et al., 2015; Zhang et al., 2007a).

More than thirty oil fields (e.g., Dawanqi, Lunnan, Tahe, Tazhong, Hetian and Bashituo) have been discovered throughout the Tarim Basin during the past three decades (Xu et al., 2004; Zhao et al., 2004). More recently discovered is the deeply buried (>6000 m) (>19,685 ft) Early Paleozoic carbonate Yijianfang Formation in the Halahatang depression of the northern Tarim Basin that has a current estimated reserve of >4 Bbbls of oil (Zhu et al., 2013a), which supports the reported resource potential within the Tarim Basin (Li, 2009; Xu et al., 2004). However, both the source and timing of hydrocarbon generation and accumulation in the Tarim Basin remain debated (Chang et al., 2013a; Li, 2009; Li et al., 2010; Liao et al., 2010; Tian, 2005; Xiao et al., 2012). Hydrocarbon maturation models propose that the Neoproterozic and Early Cambrian shales are the main source for the Shaya Uplift oilfield in the northern Tarim Basin (Li, 2009) and the Late Cambrian to Ordovician shales are the suggested oil source in Kongquehe area in northeast Tarim Basin (Tian, 2005). Based on both biomarker and $\delta^{13}C$ analysis of individual *n*-alkanes for oils, a mixed origin (Cambrian–Lower Ordovician and Middle-Upper Ordovician) has been proposed for the central Tarim Basin (Li et al., 2010). Basin modeling in the Caohu Depression in the northern Tarim Basin considers the Early Ordovician (ca. 400 Ma) to be a key time of oil generation and migration (Tian, 2005). This is, in part, supported by authigenic illite K-Ar dating (ca. 380 Ma) from the Late Silurian sandstone reservoir in the central Tarim Basin (Zhang et al., 2004). However, younger migration ages are also proposed in the central and northern Tarim Basin by authigenic illite K-Ar dates of ca. 250 and ca. 20 Ma (Zhang et al., 2004; Zhu et al.,

2013c).

In the newly discovered Halahatang oil field, previous GC-MS (terpane and sterane characteristics) analysis on the oil and potential source rocks invoke both the shales of the Cambrian Yuertusi Formation, as well as Middle-Late Ordovician carbonates of the Lianglitage and Sangtamu Formations as the main sources of the petroleum (Chang et al., 2013a; Lu et al., 2008; Xiao et al., 2016; Zhu et al., 2013a). The current burial history models and fluid inclusion data propose several age models for the petroleum evolution in the Halahatang oil field (e.g., Late Silurian, Late Permian and Neogene) (Chang et al., 2013a; Si, 2013; Xiao et al., 2012; Zhu et al., 2013a). As a result the following key aspects of the petroleum systems are debated: (1) the source(s) of the oil; (2) the timing of oil generation, and (3) the timing of oil charging within the Tarim Basin.

Rhenium-osmium (Re-Os) isotope analysis on hydrocarbons has shown potential to determine the absolute timing of hydrocarbon generation (Cumming et al., 2014; Finlay et al., 2011; Ge et al., 2016; Ge et al., 2018a; Ge et al., 2018b; Georgiev et al., 2016; Lillis and Selby, 2013; Selby and Creaser, 2005; Selby et al., 2007). Further, authigenic illite K-Ar (Ar-Ar) dating from the oil reservoir and fluid inclusion studies can help record the timing of oil migration and reservoir filling (Guo et al., 2012; Hamilton et al., 1989; Lee et al., 1985; Mark et al., 2010; Zhang et al., 2004). In this study, we apply and discuss new oil geochemical analysis, fluid inclusion analysis, and Re-Os geochronology along with previous published sandstone authigenic illite K-Ar dating (Zhang and Luo, 2011; Zhu et al., 2012), to quantitatively determine the petroleum evolution (timing of oil generation, migration/accumulation) associated with the Halahatang oilfield of the northern Tarim Basin. In addition, this work demonstrate this combined approach can

yield quantitative data to establish the timing for petroleum evolution that may aid in the further understanding of both the temporal and spatial evolution of hydrocarbon systems worldwide.

2 Geological setting

The Halahatang depression occupies an area of ~40,000 km^2 (15,444 mi^2) within the centre of the Tabei Uplift in the northern Tarim Basin (Zhu et al., 2011). The Halahatang depression is bordered by the Yingmaili, Luntai, and Lunnan Uplift to the west, north and east, respectively, and the North Depression to the south (Fig. 1C). The geology of the Halahatang depression is characterized by a thick sequence of Cambrian to Quaternary strata (~14 km) (~8.7 mi) (Fig. 2) (Jia and Wei, 2002; Zhang and Huang, 2005). The Cambrian to Ordovician strata (~4.5 km) (~2.8 mi) comprise shallow marine to lagoonal carbonates (Jia and Wei, 2002), with the Silurian to Devonian strata being represented by ~1 km (~0.62 mi) of fine-grained red beds and sandstones (Zhang and Huang, 2005), and the Carboniferous to Permian section is characterized by a ~1 km (~0.62 mi) thick interval of sandstone and mudstone (Chang et al., 2013b). Since the Triassic the renewed subsidence of the Halahatang depression has led to the accumulation of ~6 km (3.73 mi) of Mesozoic to Cenozoic fluvio-lacustrine sediments (Zhang and Huang, 2005).

The Halahatang depression records multiple tectonic events. The Late Ordovician Caledonian Orogeny resulted in the uplift of the northern and central parts of the Tarim Basin (Zhang et al., 2007a). The region encompassing the Halahatang depression existed as a marginal foreland basin until the Late Permian (Jia and Wei, 2002; Wei et al., 2000; Zhu et al., 2011), and suffered uplift during the Hercynian Orogeny (Jia and Wei, 2002).

Since the Triassic the Halahatang depression experienced several burial and uplift events controlled by the closure of the Tethys Ocean and collision between Indian and Eurasian Plates (Yanshan and Himalayan orogenies) (Jia and Wei, 2002; Xu et al., 2016; Zhang and Huang, 2005; Zhu et al., 2011).

In the Halahatang depression, the carbonates of the Middle Ordovician Yijianfang Formation (>6,000 m deep) (>19,685 ft deep) is the main hydrocarbon reservoir, with Silurian and Triassic sandstones also considered as potential reservoir units (Zhu et al., 2013a) (Fig. 2). The source rock for the oil is still debated, but the main sources are considered to be the shales of the Cambrian Yuertusi Formation, and organic-rich carbonates of the Middle to Late Ordovician Lianglitage and Sangtamu formations (Chang et al., 2013b; Cui et al., 2009; Huo et al., 2016; Xiao et al., 2016). The dense shale or mudstone above the reservoirs are considered the cap rocks (Zhang and Huang, 2005; Zhu et al., 2013a).

3 Samples and methods

Five oil samples from separate wells (Ha9, Ha11, Ha15-2, Ha701 and XK4-3) in the Halahatang depression were collected for GC-MS and Re-Os analysis (Fig. 1C). All the oil samples are from the Middle Ordovician Yijianfang Formation between ~6550m (21,489 ft) and 6850 m (22,474 ft) (Table 1). The oil physical property and organic compositions were collected from the unpublished reports of the Tarim Oil and Gas Company. The experiments were conducted at Research Institute of Petroleum Exploration and Development, PetroChina, Beijing with the oil density, oil viscosity and oil fractions measured following three different national standard methods (General

Administration of Quality Supervision Inspection and Quarantine of the People's Republic of China, 2011; National Development and Reform Commission, 2008; National Energy Administration of the People's Republic of China, 1993). The oil density, viscosity, and API values are 0.83 - 0.10, 3.15 - 342.3, and 8.46 - 38.37, respectively. The organic compositions, wax, sulfur, saturate, aromatic, resin, and asphaltene of the oil are ~6.0 %, ~0.6 %, ~56.1 %, ~16.5 %, ~4.7 %, and ~18.7 %, respectively. All the oil samples, with the exception of the oil from Well Ha701, are characterized by low viscosity (<0.90), a high API value (>29), and low asphaltene content (<25 %) (Table 1). Thus all the oils are characterized as light crude oil. However, the oil from well Ha701 possesses a high viscosity (~342) and asphaltene content (~34 %) and low API value (8.46) (Table 1), which characterizes the oil as heavy oil (Schenk et al., 2006; Zhang et al., 1990).

The gas chromatography mass spectrometry (GC-MS) analysis of the oil samples were conducted at the China University of Geoscience (Wuhan) following the analytical procedure of (Zhang et al., 2015). Approximately 30 mg of crude oil sample was dissolved in 50 ml of *n*-hexane and left for 12 hrs at room temperature. The solution was then filtered, with all the filtrates collected and evaporated under nitrogen gas to 0.5 ml. A chromatographic column (30 cm × 10 mm in diameter) was prepared using a mixed stationary phase of activated silica gel and alumina with a ratio of 3:2 (Yang et al., 2009). The concentrated sample was transferred to the chromatographic column for further separation. The saturated hydrocarbon fraction was eluted with *n*-hexane (25 ml). The fractions were then carefully concentrated under nitrogen flow to 0.5 ml with the concentration around 5-10 mg/ml for GC-MS analysis. The GC-MS system consists of

195 the Agilent 7890 GC and 5975C mass spectrometers. A DB-5MS column 50 m × 0.25
196 mm × 0.25 μm was used. High purity helium (99.9995 %) was used as a carrier gas with
197 a flow rate of 1.0 ml/min. The injector temperature was 300 ºC. The injection volume
198 was 1.0 μl. All injections were done with a 7683B series autosampler. The oven
199 temperature was programmed from 50 ºC (1 min hold) to 100°C at 10°C /min, and then
200 to 310°C (20 min hold) at 2°C /min. The mass spectrometer was operated in the electron
201 impact mode (70 eV). The temperature of ion source and transfer-line were set at 230°C
202 and 300°C, respectively. The scanned mass range was from 50 to 550 u. The temperature
203 of the quadrupole was held at 150°C.
204 For the oil Re-Os analysis, the asphaltene fraction was analyzed as Re and Os are
205 predominantly contained within the asphaltene fraction of oil (Cumming et al., 2014;
206 Georgiev et al., 2016; Lillis and Selby, 2013; Rooney et al., 2012; Selby et al., 2007). The
207 asphaltene fraction was precipitated from the oil using 40 times volume of *n*-heptane
208 (~1g oil with 40 ml solvent) at room temperature for at least 8 hrs. The Re and Os
209 isotopic compositions and abundances of the asphaltene from the oil were analysed at the
210 Laboratory for Source Rock and Sulfide Geochronology and Geochemistry and the
211 Arthur Holmes Laboratory (members of the Durham Geochemistry Centre) at Durham
212 University following published analytical procedures (Selby et al., 2005; Selby et al.,
213 2007). Approximately 100-200 mg of asphaltene were dissolved and equilibrated with a
214 known amount of a mixed ^{185}Re and ^{190}Os spike solution by inverse *aqua-regia* (3 ml
215 HCl and 6 ml HNO_3) in a Carius tube for 24 hours at 220˚C. Osmium was isolated and
216 purified from the inverse *aqua-regia* by $CHCl_3$ solvent extraction at room temperature
217 and micro-distillation. The Re was isolated using HCl-HNO_3-based anion

chromatography. The purified Re and Os were loaded on Ni and Pt filaments, respectively, and analyzed using negative ion thermal ionization mass spectrometry (NTIMS). Total procedural blanks for Re and Os are 1.60 ± 0.03 pg and 0.05 ± 0.01 pg, respectively, with an average $^{187}Os/^{188}Os$ ratio of 0.22 ± 0.06 (1 SD; n = 4). All uncertainties include the propagated uncertainty in sample and tracer solution weights, the standard, spike calibrations, mass spectrometry measurements, and blanks. In-house Re (Restd) and Os (DROsS) solutions were analyzed as a monitor of reproducibility of isotope measurements. The $^{187}Os/^{188}Os$ values of the Os standard solution DROsS during this study are 0.1611 ± 0.0004 (1SD, *n* = 126), with the $^{185}Re/^{187}Re$ values of the Re standard solution being 0.5989 ± 0.0019 (1SD, *n* = 116). These values are in agreement with those previously published for DROsS and Restd (Cumming et al., 2014; Finlay et al., 2011, 2012; Lillis and Selby, 2013; Nowell et al., 2008). The Re–Os data of this study are regressed using the program *Isoplot* V. 4.15 (Ludwig, 2003) with ^{187}Re decay constant of $1.666\times10^{-11}a^{-1}$ (Smoliar et al., 1996). The input data contains $^{187}Re/^{188}Os$ and $^{187}Os/^{188}Os$ ratios with their total absolute 2σ level uncertainty and the associated error correlation, Rho (Ludwig, 1980).

A doubly polished fluid inclusion wafer (~100 micron thick) of a bioclastic limestone from the Ordovician Yijianfang Formation from well Ha9 was prepared for the fluid inclusion studies (Fig 3). Fluid inclusion petrography, microthermometry, laser raman microspectroscopy (LRM) and confocal scanning laser microscopy (CSLM) were conducted by CV Associés Engineering, Nancy, France.

Fluid inclusion petrography was carried out using a Zeiss Axiovert 200 microscope equipped with both transmitted white and incident ultraviolet light (UV) (λ = 365 nm). A

calibrated Linkam MDS 600 heating and cooling stage was used for microthermometry. Homogenization temperatures (Th) were obtained using the thermal cycling method with a heating rate of 10 ºC/min (Goldstein and Reynolds, 1994). The measured temperature precision for the Th is ± 0.1 ºC. The LRM analyses of aqueous fluid inclusions were performed on a Labram Jobin Yvon spectrometer, using 514.5 nm radiation produced by an argon laser. The salinity of aqueous fluid was estimated by LRM following the method described by (Dubessy et al., 2002). The CSLM methodology was used to measure the gas/oil volume ratio (Fv) of the hydrocarbon inclusions previously identified by UV-fluorescence and characterized by microthermometry. The measurements were carried out using a Bio-Rad (Zeiss) Radiance 2100 Rainbow confocal scanning laser microscope equipped with an argon laser emitting at 488 nm and mounted on a Nikon TE2000-U inverted microscope.

4 Results

4.1 GC-MS analysis

Abundant biomarkers (e.g., alkane and isoprenoids, terpane and steroids) were detected in all five oil samples (Table 2). The saturate fraction gas chromatograms (SFGCs) for three of the oils (Ha9, Ha701, XK4-3) exhibit an unresolved complex mixture (UCM) (Fig. 4), however, abundant alkane compounds are still detected in the oil samples above the UCM (Fig. 4). The carbon number of the alkane distributed between $n\mathrm{C}_{12}$ and $n\mathrm{C}_{27}$, with the highest peak occurring at $n\mathrm{C}_{15}$ or $n\mathrm{C}_{16}$ (Fig. 4). For the isoprenoids, the Pristane (Pr)/Phytane(Ph) ratios of the five oil samples range between 0.68 and 0.97. The ratios of Pr/$n\mathrm{C}_{17}$ and Ph/$n\mathrm{C}_{18}$ range from 0.04 - 0.47 and 0.07- 0.64, respectively (Table 2)(Fig.

5A, B). Tricyclic terpanes, tetracyclic terpanes and hopanes were detected in the oil samples (*m/z* 191) (Fig. 4). The tricyclic terpanes range from C_{19} to C_{30}, with a clear abundance increase between C_{20}, C_{21}, and C_{23} compounds (Fig. 4). The C_{24} tetracyclic terpane (C_{24}TET) is detected in the oils. The ratios of C_{19}/C_{23} tricyclic terpane (C_{19}TT/C_{23}TT), and C_{24} tetracyclic / C_{26} tricyclics terpane (C_{24}TET/ C_{26}TT) are respectively 0.12 to 0.20 and 0.42 to 0.49 (Table 2)(Fig. 5C). The hopanes range from C_{27} to C_{35} and exhibit the highest peaks at either C_{29} or C_{30}. The hopanes show a decrease in the abundance with increasing carbon number between C_{31} and C_{35} (Fig. 4). Additional compounds (e.g., C_{30} diahopane (C_{30}DH), Ts (18α(H)-trisnorhopane), Tm (17α(H)-trisnorhopane), gammacerane and 25-nor-hopane) are also detected. The Ts/(Ts+Tm) and C_{30}DH/C_{30}H (C_{30} hopane) ratios vary from 0.37 to 0.55 (except for Ha15-2 which has a value of ~0.03) and 0.03 to 0.13, respectively (Table 2)(Fig. 5D). The gammacerane/C_{30}H ratio varies from 0.05 to 0.19, with an average of 0.12, and the 25-nor-hopane/C_{30}H ratios range from 0.15 to 2.61 (Table 2)(Fig. 5F). Sterane compounds, such as C_{21} pregnane (C_{21}P), C_{22} homopregnane (C_{22}HP), diasterane, and C_{27}-C_{29} sterane are detected (Fig. 4). The ratio of pregnane/homopregnane (C_{21}P/C_{22}HP) ranges from 2.98 to 5.69, with an average of 4.03. The C_{27}, C_{28}, C_{29} sterane content of all the oil samples present a similar V-shape distribution, which display ~50.2, 14.6 and 35.1 %, respectively, with C_{27} sterane exhibiting the greatest abundance. The ratio of C_{29}ααα 20S/(20S+20R) and C_{29}ββ/(ββ+αα) vary from 0.30 to 0.48 and 0.55 to 0.58 (Fig. 5E).

4.2 Fluid inclusion analysis

The fluid inclusion wafer from well Ha9 is composed of grains (mainly ooids, echinoderms and mollusks) enclosed by micrite and coarse calcite cements. Fluid

inclusions in both the cement and calcite replaced grains were studied. The majority of the hydrocarbon and aqueous inclusions are distributed along annealed microfractures both in the calcite cements and the calcite replaced grains. Hydrocarbon-bearing inclusions (typically ≤ 5µm wide and ~2 to 10 µm long; Fig. 3) are liquid-rich, two-phase (L+V; L>V) inclusions that display blue, green and yellow UV fluorescence and are brown in transmitted light. Some localized inclusions within the same crystal possess highly variable liquid/vapor ratio indicating late alteration events (leakage and/or necking down) (Table 3).

The majority of the aqueous inclusions are two-phase liquid rich inclusions (L+V; L>V) (Fig. 3). Rare monophase liquid-rich aqueous inclusions were also encountered. All the fluid inclusions are ≤ 5µm wide and ~2 to 15 µm long. Both aqueous and hydrocarbon inclusions commonly occur along the same annealed microfractures indicating a coeval relationship between the fluids.

The homogenization temperatures (Th) values of the hydrocarbon-bearing inclusions range from 24.6 to 122 ºC (Table 3), with the majority homogenizing between 24.6 and 79.9 ºC (Fig. 6A). The aqueous inclusions homogenize between 61.2 and 141.0 ºC (Fig. 6A). The aqueous inclusions that are coeval with the hydrocarbon-bearing inclusions homogenize between 61.2 and 102.3 ºC, with a mean Th of 82.1 ºC (Fig. 6A). The calculated salinities obtained using the method of Dubessy et al., 2002) vary from 6.7 to 20.4 wt. % NaCl eq. (Table 3), with the majority yielding values between 12 and 16 wt. % NaCl eq. The coeval hydrocarbon and aqueous inclusions have salinity values between 8.6 and 15.1 wt. % NaCl eq (Fig. 6B).

The gas/oil volume ratio (Fv) measured by confocal scanning laser microscopy (CSLM)

of three hydrocarbon-bearing inclusions, (ranging in size between 22 and 302 μm^3), ranges from 5.1 to 10.9 %. The bubble and bulk volumes of the hydrocarbon inclusions range between 1.8 and 5.6 μm^3, and 22.0 and 84.4 μm^3 (Table 3). In general, a positive relationship exists between the Th and Fv data (Fig. 6C).

LRM analysis was conducted on 14 aqueous inclusions. One coeval aqueous inclusion with a Th of 83.2 ºC (similar to the mean data, 82.1 ºC) was characterized and used for the estimation of trapping conditions of both aqueous and hydrocarbon fluids (Table 3, Fig. 7C). The CH_4 content and salinity measurement were performed on 11 aqueous inclusions in calcite. Only two samples possess CH_4 above the detection limit (0.017 and 0.075 molal) (Table 3). Both aqueous inclusion thermodynamic (AIT) modeling using the CH_4-H_2O-NaCl system (Duan et al., 1992; Guillaume et al., 2003), and hydrocarbon bearing fluid inclusion thermodynamic (PIT) modeling were used to estimate aqueous and hydrocarbon fluid trapping conditions (Montel, 1993; Pironon, 2004) in well Ha9 in the Halahatang oilfield (Fig. 7C).

4.3 Re-Os analysis

The asphaltene Re and Os abundances of the five oil samples vary between 0.06 and 9.47 ppb, and 4.9 and 57.2 ppt, respectively (Table 4). Both the Re and Os abundances of some of the oil samples are lower than those previously reported for oil and bitumen from both hydrocarbon or metalliferous systems (Cumming et al., 2014; Finlay et al., 2011; Ge et al., 2016; Georgiev et al., 2016; Lillis and Selby, 2013; Selby et al., 2005), with most of the samples possessing higher Re and Os abundances when compared with that of the average upper crust (Re: 0.198 ppb and Os: 31 ppt) (Esser and Turekian, 1993; Rudnick and Gao, 2003).

The $^{187}Re/^{188}Os$ values of the oil range from ~78 to 1655 and exhibit a radiogenic $^{187}Os/^{188}Os$ composition of 1.48 to 4.68 (Table 4). Repeat analysis of oil samples Ha9 and Ha15-2, using a separately isolated asphaltene fraction, yield very reproducible $^{187}Re/^{188}Os$ (125.4 vs 125.2 and 1655.2 vs 1636.7) and $^{187}Os/^{188}Os$ (1.66 vs 1.74 and 2.25 vs 2.25) values, and similar Re (0.81 vs 1.23 ppb and 9.47 vs 5.86 ppb) and Os (37.4 vs 57.2 ppt and 35.2 vs 22.0 ppt) abundances (Table 4). Similar reproducibility has also been shown by previous studies (Lillis and Selby, 2013; Liu et al., 2018; Selby et al., 2005).

Collectively all the Re-Os data of all five oil samples do not yield any meaningful date (Fig. 8) as sample Ha15-2 possesses a distinct Re-Os isotope composition to the remaining four oil samples that display a positive correlation between $^{187}Re/^{188}Os$ and $^{187}Os/^{188}Os$ (Fig. 8). The Re-Os data, without sample Ha15-2, yield a Model 3 (assumes that the scatter in the degree of fit of the data is a combination of the assigned uncertainties, plus a normally distributed variation in the $^{187}Os/^{188}Os$ values (Ludwig, 2008) date of 285 ± 48 Ma (n = 5, MSWD = 6.1), with an initial $^{187}Os/^{188}Os$ composition of 1.08 ± 0.20 (Fig. 8).

5 Discussion

5.1 Oil Geochemistry of the Halahatang Oilfield

The biomarker molecular composition of an oil (*n*-alkanes, terpane, sterane) records information about its origin, maturity and alteration (Peters and Moldowan, 1993b; Wu et al., 2012; Zumberge, 1987). The carbon number of the alkane distributed between nC_{12} and nC_{27}, with the highest peak occurring at nC_{15} or nC_{16} (Fig. 4), indicating the oil is

mainly sourced from bacteria and algae (Peters et al., 2005). The ratios of Pr/nC_{17} and Ph/nC_{18} range from 0.04 - 0.47 and 0.07- 0.64, respectively (Table 2) (Fig. 5A) and indicate the oils are from marine or saline facies sourced from lower bacteria and algae (Zhang et al., 2011). The pristane/phytane (Pr/Ph) ratio is a useful parameter to establish the depositional environment of the source unit of the oil. As such, Pr/Ph values of <1.0 and >3.0 are suggested to indicate either an anoxic or oxic depositional environment, respectively (Didyk et al., 1978; Hunt, 1995; Peters et al., 2005). The Pr/Ph ratios of the Halahatang oils (0.68 - 0.97) (Fig. 5B) suggest that the oils are derived from a source unit deposited under predominantly anoxic conditions in a marine environment. The similar ratios of tricyclic terpanes (e.g., C_{23}/C_{21} tricyclic terpanes ($C_{23}TT/C_{21}TT$) (~2.05), C_{23}/C_{24} tricyclic terpanes ($C_{23}TT/C_{24}TT$)(~1.73), C_{19}/C_{23} tricyclic terpanes ($C_{19}TT/C_{23}TT$) (~0.16) and the C_{24} tertracyclic / C_{26} tricyclics terpane ($C_{24}TET/C_{26}TT$) (~0.45) (Table 2) (Fig.5C)) suggest that the oils belong to one family. The low ratios of C_{19}/C_{23} tricyclic terpane ($C_{19}TT/C_{23}TT$) (0.12 - 0.20), and C_{24} tetracyclic / C_{26} tricyclics terpane ($C_{24}TET/C_{26}TT$)(0.42 - 0.49) suggest that the oil samples are derived from a source containing marine derived organic matter (Bao et al., 2012; Peters and Moldowan, 1993a; Zumberge, 1987) (Table 2)(Fig. 5C). In addition, the similar C_{21}/C_{22} sterane ($C_{21}P/C_{22}HP$) ratio (>3.0) of the oil samples is also indicative that the oils belong to the same family (Table 2). The relative abundance of the C_{27}, C_{28}, C_{29} regular steranes are used to constrain the source types, with the C_{27} sterane being linked to a marine planktonic source and the C_{29} sterane, although they can be derived from algae, is mainly sourced from higher terrestrial plants (Peters and Moldowan, 1993a). The V-shape distribution of the C_{27}, C_{28}, C_{29} regular steranes, with C_{27} possessing the largest component on the Halahatang oils

imply that the organic matter of the source has an alga source (Fig. 4) (Peters and Moldowan, 1993a). As Ts and diahopane are more resistant to thermal stress than Tm and hopane, the Ts / (Ts+Tm) and diahopane/ hopane (C_{30}DH/C_{30}H) ratios can provide insights to the level of oil maturity, with lower ratios equating to lower levels of maturity (Lu et al., 2010; Peters and Moldowan, 1993a). The Ts / (Ts + Tm) (~0.34) and C_{30}DH/C_{30}H (~0.09) ratios of the Halahatang oil samples indicate the oils are low to moderate maturity (Table 2). The C_{29} sterane is also a vital biomarker to determine the level of hydrocarbon maturity (Brooks and Welte, 1984; Peters and Moldowan, 1993a). The value of C_{29}ααα20S/(20S+20R)(~0.43) and C_{29}ββ/(ββ+αα) (~0.57) of the Halahatang oils (Fig. 5E) equates to a vitrinite reflectance (Ro) values of ~0.8 and 0.9, and implies the oils are within the oil window maturity. The unresolved complex mixture (UCM) of the gas chromatograms shown by samples Ha9, Ha701 and XK4-3, as well as, the presence of C_{29} 25-nor-hopane, with Nor25H/C_{30}H ratios of ~0.98, indicate the Halahatang oils have suffered biodegradation (Table 2) (Fig. 5F) (Wenger and Isaksen, 2002). However, the relatively complete *n*-alkane compositions of the unresolved complex mixture indicate a second oil migration and accumulation event may have occurred in the Halahatang oilfield (Lu et al., 2008; Xiao et al., 2013; Zhu et al., 2012) (Fig. 4). In the case of the Ha15-2 oil, although the majority of biomarker parameters possess similar characteristics to the other four Halahatang oil samples, its distinct maturity (Ts / (Ts+Tm) = 0.03) and biodegradation related parameters ($C_{29}Nor_{25}H/C_{30}H$ = ~0.15) (Table 2) indicate that sample Ha15-2 may have experienced alteration after the oil reservoir formed. However, as there is no obvious UCM found and that the sample possesses the lowest $C_{29}Nor_{25}H/C_{30}H$ value (0.15) (Fig. 4), thermal degradation rather

than the biodegradation may be the main alteration mechanism. In summary, the GC-MS data show that the Halahatang oils belong to one family, derived from the same source that was deposited in a marine environment. In general, the oils are of low to moderate maturity, biodegraded, and may have experienced second hydrocarbon migration event. The organic geochemical differences of oil sample Ha15-2 indicate that some of the oil within the Halahatang oilfield may have undergone alteration after oil generation.

5.2 Petroleum evolution timing constraints of the Halahatang Oilfield

Fluid inclusions represent micron scale samples of the fluids (oil, gas and water) that migrated through and interacted with the host rocks during the evolution of a hydrocarbon system in sedimentary basins (Cooley et al., 2011). Fluid inclusion studies can play a key role in developing pressure, temperature, volume and composition models of fluid (oil and aqueous fluids) dynamics in petroliferous basins. Furthermore, fluid inclusion studies are critical to the understanding of petroleum migration and accumulation, and can help to predict the distribution of petroleum resources (Aplin et al., 1999; Bodnar, 1990; Bourdet et al., 2010; Oxtoby et al., 1995; Pironon, 2004; Teinturier et al., 2002). This study uses aqueous, and hydrocarbon bearing fluid inclusions to help elucidate the history of petroleum and aqueous fluid dynamics in the Tarim basin.

The majority of the hydrocarbon-bearing fluid inclusions of this study exhibit yellow fluorescence, however, some green, and blue fluorescing inclusions are also encountered (Fig. 3). This indicates that the majority oil in the fluid inclusions is of low maturity. Indeed, hydrocarbons of different maturity or having experienced multiple migration events commonly exhibit a range of fluorescence colors (Burruss, 1985; Chen, 2014;

McLimans, 1987; Stasiuk and Snowdon, 1997). Therefore, unlike the previous fluid inclusion results from the Yingmaili oilfield, west of the Halahatang oilfield (Zhu et al., 2013a), the fluid inclusions of this study indicate that the Halahatang oilfield experienced a complex history of hydrocarbon evolution. For example, the blue fluorescing high maturity oil in some of the hydrocarbon bearing inclusions, although uncommon, maybe related to late stage hydrocarbon migration (Guo et al., 2016; Shi et al., 2015; Su et al., 1991).

The Th-salinity bivariate plot (Fig. 6B) for the aqueous FIs defines two groups: a low Th (<100 ºC) with <15 wt % NaCl eq. fluid and a fluid with Th >110 ºC and a salinity range between ~6 and 22 wt % NaCl eq. This division may reflect at least two stages of aqueous fluid movement. The broad range in Th values of the hydrocarbon bearing inclusions (~24 - 122 ºC) may reflect post-entrapment changes to the inclusion bearing fluid. This is further supported by the positive correlation between the vapor bubble volume percent (Fv % at 20 ºC) and the Th values (Fig. 6C) (Bourdet et al., 2008). The measured inclusions with the highest Th (>100 ºC) also have the highest Fv (13.9 %) values indicating post-entrapment modification. Furthermore, homogenization temperatures can decrease due to post-entrapment thermal cracking (Okubo, 2005). In our study, the two hydrocarbon bearing inclusions with the lowest Th values (~25 ºC and 43 ºC) also possess the highest CH_4 volume (~95 and 84 μm^3, Table 3), which may indicate that some of the oils in the Halahatang oilfield have experienced thermal cracking. In general, the Th of hydrocarbon bearing fluid inclusions can also be modified by other post-entrapment events or processes e.g.: necking-down and re-equilibration (Bourdet et al., 2008; Larson et al., 1973). Therefore, the Th of the aqueous fluid

inclusions that are coeval with the hydrocarbon-bearing inclusions are used to constrain the trapping temperature of the fluid that is saturated with CH_4 (Nedkvitne et al., 1993; Visser, 1982). The isochores and isopleths for the aqueous inclusions are plotted as the dash-point lines in P-T space (Fig. 7C). For comparison, isochores are also drawn for non-coeval aqueous inclusions in Figure 7C. The aqueous inclusions coeval with the hydrocarbon-bearing inclusions display a unimodal Th distribution (~61 to 102 ºC; mean Th = 82.1 ºC, n = 23) (Fig. 7B). Two Th values were used to model the fluid trapping conditions (Fig. 7C) i.e. Th of 83.2 ºC (a coeval aqueous inclusion) the other represents the mean Th value (~82.0ºC). The solid lines in Figure 6C are the isochores (and isopleths) for the three oil bearing inclusions plotted in Figure 5C. The intersections of the isochores for the oil-bearing inclusion (solid lines, Fig. 7C) and the selected coeval aqueous inclusions provide estimated fluid trapping temperatures of 100 to 110 ºC and fluid trapping pressures of ~39 to 59 MPa (Fig. 7C).

Basin modelling coupled with fluid inclusion analysis has been widely applied to constrain the timing of hydrocarbon charging in petroleum systems (Cao et al., 2006; Guo et al., 2012; Roberts et al., 2004). In the Halahatang depression, basin modelling based on wells Ha601 and Ha9 suggest that the Early Palaeozoic source units were buried to ~3500 m (11,483 ft) and underwent hydrocarbon maturation between the Carboniferous and Permian (Zhang et al., 2007a; Zhu et al., 2012). Plotting the modelled Th data from this study with the previous basin model, one prolonged oil migration event during the Permian is proposed (Fig. 7A), which agrees with previous fluid inclusion studies of the Halahatang depression that also indicated the migration of hydrocarbons during the Late Permian (Xiao et al., 2012).

Authigenic illite is one of the last phases formed mineral cements prior to hydrocarbon migration into a sandstone reservoir (Hamilton et al., 1989). If the displacement of an aqueous pore fluid is replaced by hydrocarbons this leads to the cessation of illite formation (Lee et al., 1985). The last formed illite can be used to determine the maximum timing of hydrocarbon emplacement or migration (Hogg et al., 1993). Among the many diagenetic clay mineral products amenable for geochronology, illite is the only commonly occurring diagenetic mineral in sandstone reservoirs that contain sufficient long-lived radioisotope (^{40}K), which permit the determination of its formation age (Hamilton et al., 1989). Although there is no sandstone reservoir in the Halahatang depression, in the Yingmaili Oilfield, ~30 km (~18.6 mi) northwest of the Halahatang depression, the Silurian Keping Formation sandstone reservoir is well-developed (Li et al., 2009). This sandstone strata is a reservoir to bitumen/oil and gas (Zhang and Luo, 2011). Hydrocarbons of the Silurian Keping Formation share a similar origin to hydrocarbons reservoired in Ordovician strata and thus may have charged at the same time (Zhu et al., 2013a). Published illite K-Ar isotope data in the Keping Formation sandstone reservoir (Zhang and Luo, 2011; Zhu et al., 2012) could aid in understanding the petroleum evolution (migration) in the Halahatang oilfield. Seven sandstone samples from different wells (YM11, YM34, YM35, YM35-1) and depths (Fig. 1C) show a decreasing age trend from the northwest (293 ± 2) to the southeast (255 ± 3 Ma) (Zhang and Luo, 2011; Zhu et al., 2012). The much younger illite K-Ar date than the deposition age of the Keping Formation indicates the sandstone samples contain no or little detrital illitic contamination and that the K-Ar date obtained from the fine fraction should approximately reflect the timing of diagenetic illite formation. Except for the Yingmaili

oilfield which is near to the Halahatang oilfield, other K-Ar dates in Tarim Basin, e.g., the Hadexun oilfield in the Northern Depression and Tazhong oilfield, respectively ~50 km (~31 mi) and ~100 km (~62 mi) south to the Hahalatang depression (Fig. 1B), also possess illite K-Ar dates of ~250 Ma and ~230 Ma, respectively (Zhang et al., 2007b; Zhu et al., 2013b). All the illite K-Ar dates (~280 - 230 Ma) from the central and northern Tarim Basin coincide with the above fluid inclusion and basin modelling data that show the major hydrocarbon migration and accumulation occurred predominantly during between the Mid to Late Permian.

Petroleum evolution is a complex process including oil generation, migration and finally accumulation or destruction. Oil generation, which leads the whole evolution process, is one key factor. Previous research has shown that oil generation is a multi-step procedure involving bitumen formation from the kerogen and oil generation from the bitumen, and that these two steps are closely related (Lewan, 1985). Oil/bitumen/pyrobitumen Re-Os analysis, which is a new and challenging method, has shown potential in constraining the absolute timing of the oil/bitumen/pyrobitumen generation (Cumming et al., 2014; Finlay et al., 2011; Ge et al., 2016; Lillis and Selby, 2013; Liu et al., 2018; Selby and Creaser, 2005). Although the GC-MS analysis and fluid inclusion analysis indicate that some oil samples in this study have suffered from biodegradation and secondary migration, however, previous research has shown that biodegradation do not significantly affect the Re-Os systematics of oil (Lillis and Selby, 2013). Moreover, and if the oils generated during one period, then multiple oil migration episodes following the generation will not disturb the hydrocarbon Re-Os system (Finlay et al., 2011; Lillis and Selby, 2013; Selby et al., 2005).

The Re-Os data for all oil samples, except sample Ha15-2, yield a Model 3 Re-Os age of 285 ± 48 Ma (Osi = 1.08 ± 0.20 [18.5 %], MSWD = 6.1). The large age uncertainty (~17 %) and MSWD value is beyond that associated with analytical uncertainty (~1.0), and is considered to be directly related to the variation in the initial $^{187}Os/^{188}Os$ ratio (Os_i) of the sample set (Cohen et al., 1999; Ludwig, 2008) (Fig. 8; Table 4). Given that oils are generated from a source horizon that can be both stratigraphically (10s to 100s of m/ft) and geographically (10s to 100s kilometers/miles) expansive, the ability for oil sampled across a reservoir to possess the same initial Os_i ratio can be challenged (see (Lillis and Selby, 2013)), but can also exhibit a limited range in values ((Liu et al., 2018 and references therein). The variation in Os_i values could also relate to the oil sampled being associated with difference stages of the oil generation of a petroleum system (Liu et al., 2018).

The ~285 Ma Re-Os date, including its uncertainty of 48 Ma, is in good agreement with the understanding of the timing of oil generation in northern Tarim Basin (Zhu et al., 2013a; Zhu et al., 2012). Basin modelling both in the Halahatang and Yingmaili oilfields of the northern Tarim Basin, suggest that a Paleozoic source was buried to ~3000 m (~9842 ft) and underwent hydrocarbon maturation during the Late Carboniferous to Early Permian (Zhu et al., 2013a; Zhu et al., 2012). Although possessing a relatively large uncertainty (48 Ma), the ~285 Ma Re-Os date, which is nominally slightly older than the oil migration / accumulation timing constrained by basin modelling coupled with fluid inclusion analysis and the reservoir illite K-Ar dates (see above), suggests that the Re-Os date represents the best absolute estimate for the timing of oil generation in the Halahatang oilfield.

The oil sample Ha15-2 plots to right of the defined best-fit line (isochron) of the bulk of the Re-Os data for the oil sample set (Fig. 8). In comparison to the other oil samples, sample Ha15-2 also possesses different parameters in biomarker analysis ($C_{29}NOR_{25}H/C_{30}H$ = 0.15, Ts/(Ts+Tm) = 0.03) indicating the sample has experience post-generation alteration. Furthermore, although of limited abundance, the presence of oil-bearing fluid inclusions with high Th (>120 ºC) and a CH_4 volume of ~ 90 μm^3 of this study (Table 3) also indicate thermal cracking may have occurred in regions in the Halahatang oilfied. Moreover, the basin modelling shows that the Paleozoic strata in this area have been buried to ~7000 m (~ 22,966 ft) since the Late Neogene (Fig. 7A) (Zhu et al., 2012), and that during the last ~10 Myrs the high temperatures (>150ºC) may have led to thermal cracking of oil, particular in deeper parts, of the Halahatang oilfield (eg, Ha 15-2 oil). Previous work on TSR affected oil from the Manderson, South of the Bighorn Basin (Lillis and Selby, 2013) and pyrobitumen from Majiang - Wanshan reservoir, South China (Ge et al., 2016) have shown that the high temperature controlled thermal cracking can reset the Re-Os systematics in the hydrocarbons (oil/bitumen). The high Th and CH_4 volume evidence from fluid inclusions, and basin modelling suggest that the thermal cracking which could lead to gas formation (Hill et al., 2003; Huc et al., 2000) may have resulted in the Re-Os characteristics shown by oil sample Ha15-2. Additional research on similar oils to Ha15-2 from the Halahatang oilfield will be necessary to see if the Re-Os systematics are still being effected by thermal cracking as it has been suggested the closure temperature of Re-Os in thermal cracked oil is ≤120˚C (Ge et al., 2016; Lillis and Selby, 2013).

5.3 Petroleum evolution in the Halahatang depression

563 Based on the general tectonic evolution of the Tarim Basin, and combining the oil Re-Os
564 dating and fluid inclusion analysis of this study from the Halahatang depression, and
565 previous basin modeling and illite K-Ar isotope dates from Tarim Basin, the petroleum
566 evolution in the Halahatang depression can be summarized as follows. Exhumation of
567 Silurian strata driven by the Caledonian Orogeny during the Devonian (Fig. 9A) (Lin et
568 al., 2015), the Tarim Basin transferred into an extensional environment between the
569 Carboniferous and Permian (Zhang et al., 2007a). The continued subsidence during this
570 period led to the burial (>3500 m) (>11483 ft) of the Paleozoic source units (Cambrian to
571 Ordovician shales/mudstone) and oil generation during the Early Permian (Fig. 9B)
572 (~285 Ma Re-Os oil date). The closure of the Tian Shan Sea (Late Hercynian tectonic
573 event) caused a phase of uplift and exhumation during the Mid-Late Permian that resulted
574 in the cessation the oil generation (Lin et al., 2015; Zhang et al., 2007a). However,
575 tectonic instability, as well as, the simultaneous formed faults provided pathways for oil
576 migration and accumulation (Zhu et al., 2013c). Both basin modelling and coupled fluid
577 inclusion analysis of this study and previous illite K-Ar dating (~280 - 230 Ma) within
578 central and northern Tarim Basin (Zhang et al., 2007b; Zhang and Luo, 2011; Zhu et al.,
579 2012; Zhu et al., 2013b) show that hydrocarbon migration and accumulation occurred
580 predominantly during the Mid-Permian, but also during the Early Triassic (Fig. 9C). The
581 Tarim Basin changed to a continental sedimentary depositional environment as of the
582 Mesozoic (Zhang and Huang, 2005). The basin burial history of the Halahatang
583 depression shows a continuous sedimentary deposition since the Late Triassic including a
584 rapid sedimentation since the Neogene (Fig. 9D). This has resulted in the deep burial
585 (~7000 m) (22965 ft) of the Ordovician reservoirs. The deep burial and high temperatures

(>150 ºC) are suitable for oil cracking to occur. Both the high Th and CH_4 volume observed in oil-bearing fluid inclusion and the oil Re-Os isotope characteristics of Ha 15-2 oil show evidence of thermal cracking in parts of the Halahatang oilfiled. However, the organic geochemistry (Fig. 4) (Table 2), fluid inclusion analysis (Fig. 3) (Table 3) and Re-Os data (Fig. 8) of this study suggests that thermal cracking of oil in the Halahatang depression is neither prolonged nor widespread.

6 Conclusions

Combining the organic geochemical analysis, fluid inclusion analysis and Re-Os isotope analysis of the Halahatang oilfiled, in addition to previously published basin modeling and illite K-Ar dating in Tarim Basin, the petroleum evolution of the Halahatang oilfield, Northern Tarim Basin is quantitatively constrained. The organic geochemistry analyses show the oil samples belong to same family, with the oils derived from a source deposited in an anoxic marine environment, possess low to middle maturity and have undergone limited biodegradation. The ~285 Ma Re-Os date coincides with the hydrocarbon trap evolution, the Cambrian-Ordovician source rock maturation history (Zhang et al., 2007a), basin modelling result for the Halahatang depression, and the nearby Yingmai Basin indicating that the Re-Os data records the timing of oil generation. Traditional basin modelling coupled with fluid inclusion analysis are in good agreement with published illite K-Ar dates (280 - 230 Ma) (Zhang et al., 2007b; Zhang and Luo, 2011; Zhu et al., 2012; Zhu et al., 2013b) in the Tarim basin and suggest that oil migration/accumulation occurred during the Mid-Permian to Early Triassic. The Re-Os geochemistry of Ha15-2, and oil-bearing fluid inclusion analysis suggest that some oils in

609 the Halahatang depression have experienced thermal cracking since the Neogene.

610 Integrating fluid inclusion analysis, reservoir illite K-Ar dating and Re-Os oil analysis,
611 this work quantitatively establishes the entire petroleum evolution (generation,
612 migration/accumulation) process in the Halahatang depression of the northern Tarim
613 Basin. In addition to Tarim basin, the coupled analysis of Re-Os oil geochronology with
614 K-Ar dating and fluid inclusions is also applicable to petroleum systems worldwide to aid
615 in the understanding of both the temporal and spatial evolution of hydrocarbon systems.

616 **References**

617 Aplin, A., G. Macleod, S. Larter, K. Pedersen, H. Sorensen, and T. Booth, 1999, Combined use of
618 Confocal Laser Scanning Microscopyand PVT simulation for estimating the composition
619 andphysical properties of petroleum in fluid inclusions: Marine and Petroleum Geology, v. 16,
620 p. 97-110, Doi. 10.1016/S0264-8172(98)00079-8.
621 Bao, J., J. Kong, C. Zhu, Q. Zhang, M. Li, Y. Lu, and W. Zhang, 2012, Geochemical Characteristics of a
622 Norvel Kind of Marine Oils from Tarim Basin: Acta Sedimentologica Sinica, v. 30, p. 580-587,
623 Doi. 10.14027/j.cnki.cjxb.2012.03.009.
624 Bodnar, R. J., 1990, Petroleum Migration in the Miocene Monterey Formation, California, USA:
625 Constraints from Fluid-Inclusion Studies: Mineralogical Magazine, v. 54, p. 295-304, Doi.
626 10.1180/minmag.1990.054.375.15.
627 Bourdet, J., J. Pironon, G. Levresse, and J. Tritlla, 2008, Petroleum type determination through
628 homogenization temperature and vapour volume fraction measurements in fluid inclusions:
629 Geofluids, v. 8, p. 46-59, Doi. 10.1111/j.1468-8123.2007.00204.x.
630 Bourdet, J., J. Pironon, G. Levresse, and J. Tritlla, 2010, Petroleum accumulation and leakage in a
631 deeply buried carbonate reservoir, Níspero field (Mexico): Marine and Petroleum Geology, v.
632 27, p. 126-142, Doi. 10.1016/j.marpetgeo.2009.07.003.
633 Brooks, J., and D. Welte, 1984, Advances in petroleum geochemistry, Academic Press, 344 p.
634 Burruss, R. C., 1985, Timing of hydrocarbon migration: evidenced from fluid inclusions in calcite
635 cements, tectonics and burial history: Harris, P.M. (Ed.), Carbonates Cements. Society of
636 Economic Paleontologists and Mineralogists Special Publication, v. 26, p. 277-289, Doi.
637 10.2110/pec.85.36.0277.
638 Cao, J., S. Yao, Z. Jin, W. Hu, Y. Zhang, X. Wang, Y. Zhang, and Y. Tang, 2006, Petroleum migration and
639 mixing in the northwestern Junggar Basin (NW China): constraints from oil-bearing fluid
640 inclusion analyses: Organic Geochemistry, v. 37, p. 827-846, Doi.
641 10.1016/j.orggeochem.2006.02.003.
642 Chang, X., T.-G. Wang, Q. Li, B. Cheng, and X. Tao, 2013a, Geochemistry and possible origin of
643 petroleum in Palaeozoic reservoirs from Halahatang Depression: Journal of Asian Earth
644 Sciences, v. 74, p. 129-141, Doi. 10.1016/j.jseaes.2013.03.024.
645 Chang, X., T. G. Wang, L. Qiming, and O. Guangxi, 2013b, Charging of Ordovician reservoirs in the
646 Halahatang depression (Tarim Basin, NW China) determined by oil geochemistry: Journal of
647 Petroleum Geology, v. 36, p. 383-398, Doi. 10.1111/jpg.12562.
648 Chen, H., 2014, Microspectrofluorimetric characterization and thermal maturity assessment of
649 individual oil inclusion: Acta Petrolei Sinica, v. 35, p. 584-590, Doi. 10.7623/syxb201403023.
650 Cohen, A. S., A. L. Coe, J. M. Bartlett, and C. J. Hawkesworth, 1999, Precise Re–Os ages of organic-rich
651 mudrocks and the Os isotope composition of Jurassic seawater: Earth and Planetary Science
652 Letters, v. 167, p. 159-173, Doi. 10.1016/S0012-821X(99)00026-6.

Cooley, M. A., R. A. Price, T. K. Kyser, and J. M. Dixon, 2011, Stable-isotope geochemistry of syntectonic veins in Paleozoic carbonate rocks in the Livingstone Range anticlinorium and their significance to the thermal and fluid evolution of the southern Canadian foreland thrust and fold belt: AAPG Bulletin, v. 95, p. 1851-1882, Doi. 10.1306/01271107098.

Cui, H., D. Zheng, and T. Teng, 2009, Petroleum geologic characteristics and exploration orientation in Halahatang Depression of Tabei uplift: Lithologic Reservoirs v. 21, p. 54-58.

Cumming, V. M., D. Selby, P. G. Lillis, and M. D. Lewan, 2014, Re–Os geochronology and Os isotope fingerprinting of petroleum sourced from a Type I lacustrine kerogen: Insights from the natural Green River petroleum system in the Uinta Basin and hydrous pyrolysis experiments: Geochimica et Cosmochimica Acta, v. 138, p. 32-56, Doi. 10.1016/j.gca.2014.04.016.

Didyk, B. M., B. R. T. Simoneit, S. C. Brassell, and G. Eglinton, 1978, Organic geochemical indicators of palaeoenvnonmental conditions of sedimentation: Nature, v. 272, p. 216-222, Doi. 10.1038/272216a0.

Duan, Z., N. Møller, J. Greenberg, and J. H. Weare, 1992, The prediction of methane solubility in natural waters to high ionic strength from 0 to 250°C and from 0 to 1600 bar: Geochimica et Cosmochimica Acta, v. 56, p. 1451-1460, Doi. 10.1016/0016-7037(92)90215-5.

Duan, Z., and S. Mao, 2006, A thermodynamic model for calculating methane solubility, density and gas phase composition of methane-bearing aqueous fluids from 273 to 523 K and from 1 to 2000 bar: Geochimica et Cosmochimica Acta, v. 70, p. 3369-3386, Doi. 10.1016/j.gca.2006.03.018.

Dubessy, J., T. Lhomme, M.-C. Boiron, and F. Rull, 2002, Determination of Chlorinity in Aqueous Fluids Using Raman Spectroscopy of the Stretching Band of Water at Room Temperature: Application to Fluid Inclusions: Applied Spectroscopy, v. 56, p. 99-106, Doi. 10.1366/0003702021954278.

Esser, B. K., and K. K. Turekian, 1993, The osmium isotopic composition of the continental crust: Geochimica et Cosmochimica Acta, v. 57, p. 3093-3104, Doi. 10.1016/0016-7037(93)90296-9.

Finlay, A. J., D. Selby, and M. J. Osborne, 2011, Re-Os geochronology and fingerprinting of United Kingdom Atlantic margin oil: Temporal implications for regional petroleum systems: Geology, v. 39, p. 475-478, Doi. 10.1130/G31781.1.

Finlay, A. J., D. Selby, and M. J. Osborne, 2012, Petroleum source rock identification of United Kingdom Atlantic Margin oil fields and the Western Canadian Oil Sands using Platinum, Palladium, Osmium and Rhenium: Implications for global petroleum systems: Earth and Planetary Science Letters, v. 313, p. 95-104, Doi. 10.1016/j.epsl.2011.11.003.

Ge, X., C. Shen, D. Selby, D. Deng, and L. Mei, 2016, Apatite fission-track and Re-Os geochronology of the Xuefeng uplift, China: Temporal implications for dry gas associated hydrocarbon systems: Geology, v. 44, p. 491-494, Doi. 10.1130/g37666.1.

Ge, X., C. Shen, D. Selby, G. Wang, Z. Yang, Y. Gong, and S. Xiong, 2018a, Neoproterozoic-Cambrian petroleum system evolution of the Micang Shan Uplift, Northern Sichuan Basin, China : insights from pyrobitumen Re-Os geochronology and apatite fission track analysis: AAPG Bulletin, v. 102, p. 1429-1453, Doi. 10.1306/1107171616617170.

Ge, X., C. Shen, D. Selby, J. Wang, L. Ma, X. Ruan, S. Hu, and L. Mei, 2018b, Petroleum generation timing and source in the Northern Longmen Shan Thrust Belt, Southwest China: Implications for multiple oil generation episodes and sources: AAPG Bulletin, v. 102, p. 913-938, Doi. 10.1306/0711171623017125.

General Administration of Quality Supervision Inspection and Quarantine of the People's Republic of China, 2011, Density or relative density analysis methods on crude petroleum and liquid or solid petroleum products p. 17.

Georgiev, S. V., H. J. Stein, J. L. Hannah, R. Galimberti, M. Nali, G. Yang, and A. Zimmerman, 2016, Re–Os dating of maltenes and asphaltenes within single samples of crude oil: Geochimica et Cosmochimica Acta, v. 179, p. 53-75, Doi. 10.1016/j.gca.2016.01.016.

Goldstein, R., and T. Reynolds, 1994, Systematics of fluid inclusions in diagenetic minerals: SEPM (Society for Sedimentary Geology) Short Course 31, SEPM (Society for Sedimentary Geology).

Guillaume, D., S. Teinturier, J. Dubessy, and J. Pironon, 2003, Calibration of methane analysis by Raman spectroscopy in H2O–NaCl–CH4 fluid inclusions: Chemical Geology, v. 194, p. 41-49, Doi.

10.1016/S0009-2541(02)00270-X.
Guo, X., K. Liu, S. He, G. Song, Y. Wang, X. Hao, and B. Wang, 2012, Petroleum generation and charge history of the northern Dongying Depression, Bohai Bay Basin, China: Insight from integrated fluid inclusion analysis and basin modelling: Marine and Petroleum Geology, v. 32, p. 21-35, Doi. 10.1016/j.marpetgeo.2011.12.007.
Guo, X., K. Liu, C. Jia, Y. Song, M. Zhao, Q. Zhuo, and X. Lu, 2016, Fluid evolution in the Dabei Gas Field of the Kuqa Depression, Tarim Basin, NW China: Implications for fault-related fluid flow: Marine and Petroleum Geology, v. 78, p. 1-16, Doi. 10.1016/j.marpetgeo.2016.08.024.
Hamilton, P., S. Kelley, and A. E. Fallick, 1989, K-Ar dating of illite in hydrocarbon reservoirs: Clay Minerals, v. 24, p. 215-231, Doi. 10.1180/claymin.1989.024.2.08.
Hill, R. J., Y. Tang, and I. R. Kaplan, 2003, Insights into oil cracking based on laboratory experiments: Organic Geochemistry, v. 34, p. 1651-1672, Doi. 10.1016/s0146-6380(03)00173-6.
Hogg, A., P. Hamilton, and R. Macintyre, 1993, Mapping diagenetic fluid flow within a reservoir: K-Ar dating in the Alwyn area (UK North Sea): Marine and Petroleum Geology, v. 10, p. 279-294, Doi. 10.1016/0264-8172(93)90110-E.
Huc, A. Y., P. Nederlof, R. Debarre, B. Carpentier, M. Boussafir, F. Laggoun-Défarge, A. Lenail-Chouteau, and N. Bordas-Le Floch, 2000, Pyrobitumen occurrence and formation in a Cambro–Ordovician sandstone reservoir, Fahud Salt Basin, North Oman: Chemical Geology, v. 168, p. 99-112, Doi. 10.1016/S0009-2541(00)00190-X.
Hunt, M., 1995, Petroleum geochemistry and geology, 2nd Edition: New York, NY, WH Freeman and company, 743 p.
Huo, Z., T. Jiang, X. Pang, W. Wang, J. Chen, J. Song, W. Shen, and Z. Pan, 2016, Evaluation of Deep Carbonate Source Rocks with Low TOC and Contribution to Oil-Gas Accumulation in Tazhong Area, Tarim Basin: Earth Science, v. 41, p. 2061-2074, Doi. 10.3799/dqkx.2016.143.
Jia, C., and G. Wei, 2002, Structural characteristics and petroliferous features of Tarim Basin: Chinese Science Bulletin, v. 47, p. 1-11, Doi. 10.1007/BF02902812.
Larson, L. T., J. D. Miller, J. E. Nadeau, and E. Roedder, 1973, Two sources of error in low temperature inclusion homogenization determination, and corrections on published temperatures for the East Tennessee and Laisvall deposits: Economic Geology, v. 68, p. 113-116, Doi. 10.2113/gsecongeo.68.1.113.
Lee, M., J. L. Aronson, and S. M. Savin, 1985, K/Ar dating of time of gas emplacement in Rotliegendes sandstone, Netherlands: AAPG Bulletin, v. 69, p. 1381-1385.
Lewan, M., 1985, Evaluation of petroleum generation by hydrous pyrolysis experimentation: Philosophical Transactions of the Royal Society of London. Series A, Mathematical and Physical Sciences, v. 315, p. 123-134, Doi. 10.1306/94886d71-1704-11d7-8645000102c1865d.
Li, K., 2009, The Three Main Paleohigh's Evolution and affection Hydrocarbon Accumulation, Tarim Basin, Chengdu University of Technology, 157 p.
Li, S., X. Pang, Z. Jin, H. Yang, Z. Xiao, Q. Gu, and B. Zhang, 2010, Petroleum source in the Tazhong Uplift, Tarim Basin: new insights from geochemical and fluid inclusion data: Organic Geochemistry, v. 41, p. 531-553, Doi. 10.1016/j.orggeochem.2010.02.018.
Li, Y., C. Xie, X. Deng, and H. Guo, 2009, Reservoir characteristic and controlling factors of Silurian Kepingtage Fromation in YM34 and YM35 well block: Geology in China, v. 26, p. 1087-1098.
Liao, Z., L. Zhang, C. Yang, H. Zhang, T. Wang, and Y. Lu, 2010, Geochemical characteristics of heavy oils from the east and west sides of Halahatang Depression, Tarim Basin, Chian: Exemplified by oils of LG7 and DH1-6-9: GEOCHIMICA, v. 39, p. 149-153.
Lillis, P. G., and D. Selby, 2013, Evaluation of the rhenium–osmium geochronometer in the Phosphoria petroleum system, Bighorn Basin of Wyoming and Montana, USA: Geochimica et Cosmochimica Acta, v. 118, p. 312-330, Doi. 10.1016/j.gca.2013.04.01
Lin, B., X. Zhang, X. Xu, J. Yuan, Y. Neng, and J. Zhu, 2015, Features and effects of basement faults on deposition in the Tarim Basin: Earth-Science Reviews, v. 145, p. 43-55, Doi. 10.1016/j.earscirev.2015.02.008.
Liu, J., D. Selby, M. Obermajer, and A. Mort, 2018, Re-Os geochronology and oil-source correlation of Duvernay Petroleum System, Western Canada Sedimentary Basin: Implications for the application of the Re-Os geochronometer to petroleum systems: AAPG Bulletin, v. 108, p.

763 1627-1657, Doi. 10.1306/12081717105.
764 Liu, W., J. Wang, C. Tao, G. Hu, L. Lu, and P. Wang, 2013, The Geochronology of Petroleum
765 Accumulation of China Marine Sequence: Natural Gas Geoscience, v. 24, p. 199-209.
766 Lu, J., S. Chen, X. Wang, L. Lu, X. Chen, and Y. Wang, 2010, Maturity study of the strong biodegradation
767 viscous oil: taking the Santai-Beisantai area of Junggar Basin as an example. : Petroleum
768 Geology & Experiment, v. 32, p. 373-376.
769 Lu, Y., Z. Xiao, Q. Gu, and Q. Zhang, 2008, Geochemical characteristics and accumulation of marine oil
770 and gas around Halahatang depression, Tarim Basin, China: Science in China Series D: Earth
771 Sciences, v. 51, p. 195-206, Doi. 10.1007/s11430-008-5006-0.
772 Ludwig, K., 2003, A plotting and regression program for radiogenic-isotope data, version 3.00: United
773 State Geol Survey, open file report, p. 1-70.
774 Ludwig, K., 2008, User's Manual for Isoplot 3.7: A geochronological toolkit for Microsoft Excel., v.
775 Special Publication No.4: Berkeley Geochronological Centre, 76 p.
776 Ludwig, K. R., 1980, Calculation of uncertainties of U-Pb isotope data: Earth and Planetary Science
777 Letters, v. 46, p. 212-220, Doi. 10.1016/0012-821X(80)90007-2.
778 Mark, D. F., J. Parnell, S. P. Kelley, M. R. Lee, and S. C. Sherlock, 2010, 40Ar/39Ar dating of oil
779 generation and migration at complex continental margins: Geology, v. 38, p. 75-78, Doi.
780 10.1130/G30237.1.
781 McLimans, R. K., 1987, The application of fluid inclusions to migration of oil and diagenesis in
782 petroleum reservoirs: Applied Geochemistry, v. 2, p. 585-603, Doi. 10.1016/0883-
783 2927(87)90011-4.
784 Montel, F., 1993, Phase equilibria needs for petroleum exploration and production industry: Fluid
785 Phase Equilibria, v. 84, p. 343-367, Doi. 10.1016/0378-3812(93)85132-6.
786 National Development and Reform Commission, 2008, Analysis method for fraction of rock extract
787 and crude oil p. 8.
788 National Energy Administration of the People's Republic of China, 1993, Analysis method for crude oil
789 viscosity, p. 4.
790 Nedkvitne, T., D. A. Karlsen, K. Bjørlykke, and S. R. Larter, 1993, Relationship between reservoir
791 diagenetic evolution and petroleum emplacement in the Ula Field, North Sea: Marine and
792 Petroleum Geology, v. 10, p. 255-270, Doi. 10.1016/0264-8172(93)90108-5.
793 Nowell, G., D. Pearson, S. Parman, A. Luguet, and E. Hanski, 2008, Precise and accurate 186Os/188Os
794 and 187Os/188Os measurements by multi-collector plasma ionisation mass spectrometry,
795 part II: Laser ablation and its application to single-grain Pt–Os and Re–Os geochronology:
796 Chemical Geology, v. 248, p. 394-426, Doi. 10.1016/j.chemgeo.2007.12.004.
797 Okubo, S., 2005, Effects of thermal cracking of hydrocarbons on the homogenization temperature of
798 fluid inclusions from the Niigata oil and gas fields, Japan: Applied Geochemistry, v. 20, p. 255-
799 260, Doi. 10.1016/j.apgeochem.2004.09.001.
800 Oxtoby, N. H., A. W. Mitchell, and J. G. Gluyas, 1995, The filling and emptying of the Ula Oilfield: fluid
801 inclusion constraints: Geological Society Special Publications, v. 86, p. 141-157, Doi.
802 10.1144/GSL.SP.1995.086.01.11.
803 Peters, K., C. Walters, and J. Moldowan, 2005, The Biomarker guide, biomarkers and isotopes in
804 petroleum exploration and earth history, vol 1–2, Cambridge University Press, New York, 961
805 p.
806 Peters, K. E., and J. M. Moldowan, 1993a, The biomarker guide: interpreting molecular fossils in
807 petroleum and ancient sediments, Englewood Cliffs, NJ (United States); Prentice Hall.
808 Peters, K. E., and J. M. Moldowan, 1993b, The biomarker guide: interpreting molecular fossils in
809 petroleum and ancient sediments: United States, Englewood Cliffs, NJ (United States);
810 Prentice Hall, 363 p.
811 Pironon, J., 2004, Fluid inclusions in petroleum environments: analytical procedure for PTX
812 reconstruction: Acta Petrolei Sinica, v. 20, p. 1332-1342.
813 Qiu, H.-N., H.-Y. Wu, J.-B. Yun, Z.-H. Feng, Y.-G. Xu, L.-F. Mei, and J. Wijbrans, 2011, High-precision
814 40Ar/39Ar age of the gas emplacement into the Songliao Basin: Geology, v. 39, p. 451-454,
815 Doi. 10.1130/G31885.1.
816 Roberts, L. N., M. D. Lewan, and T. M. Finn, 2004, Timing of oil and gas generation of petroleum
817 systems in the Southwestern Wyoming Province: Mountain Geologist, p. 87-117.

Rooney, A. D., D. Selby, M. D. Lewan, P. G. Lillis, and J.-P. Houzay, 2012, Evaluating Re–Os systematics in organic-rich sedimentary rocks in response to petroleum generation using hydrous pyrolysis experiments: Geochimica et Cosmochimica Acta, v. 77, p. 275-291, Doi. 10.1016/j.gca.2011.11.006.

Rudnick, R., and S. Gao, 2003, Composition of the continental crust: Treatise on geochemistry, v. 3, p. 1-64, Doi. 10.1016/0016-7037(95)00038-2.

Schenk, C., R. Pollastro, and R. Hill, 2006, Natural bitumen resources of the United States: US Geological Survey Fact Sheet, v. 3133, p. 1-2.

Selby, D., and R. A. Creaser, 2005, Direct radiometric dating of hydrocarbon deposits using rhenium-osmium isotopes: Science, v. 308, p. 1293-1295, Doi. 10.1126/science.1111081.

Selby, D., R. A. Creaser, K. Dewing, and M. Fowler, 2005, Evaluation of bitumen as a 187Re–187Os geochronometer for hydrocarbon maturation and migration: a test case from the Polaris MVT deposit, Canada: Earth and Planetary Science Letters, v. 235, p. 1-15, Doi. 10.1016/j.epsl.2005.02.018.

Selby, D., R. A. Creaser, and M. G. Fowler, 2007, Re–Os elemental and isotopic systematics in crude oils: Geochimica et Cosmochimica Acta, v. 71, p. 378-386, Doi. 10.1016/j.gca.2006.09.005.

Shi, C., J. Cao, J. Bao, C. Zhu, X. Jiang, and M. Wu, 2015, Source characterization of highly mature pyrobitumens using trace and rare earth element geochemistry: Sinian–Paleozoic paleo-oil reservoirs in South China: Organic Geochemistry, v. 83-84, p. 77-93, Doi. 10.1016/j.orggeochem.2015.03.008.

Si, S., 2013, Comparison of Characteristics of Hydrocarbon Accumulation between Bashituo and Manan Structural Belts in Markit Slope, Tarim Basin, China University of Geoscience (Wuhan).

Smoliar, M. I., R. J. Walker, and J. W. Morgan, 1996, Re-Os ages of group IIA, IIIA, IVA, and IVB iron meteorites: Science, v. 271, p. 1099-1102, Doi. 10.1126/science.271.5252.1099.

Stasiuk, L., and L. Snowdon, 1997, Fluorescence micro-spectrometry of synthetic and natural hydrocarbon fluid inclusions: crude oil chemistry, density and application to petroleum migration: Applied Geochemistry, v. 12, p. 229-241, Doi. 10.1016/S0883-2927(96)00047-9.

Su, A., K. Cheng, and W. Jin, 1991, Applications of microscopic fluorescent analysis of source rock slices on primary migation of petroleum Petroleum Exploration and Development, v. 18, p. 19-24.

Teinturier, S., J. Pironon, and F. Walgenwitz, 2002, Fluid inclusions and PVTX modelling: examples from the Garn Formation in well 6507/2-2, Haltenbanken, Mid-Norway: Marine and Petroleum Geology, v. 19, p. 755-765, Doi. 10.1016/S0264-8172(02)00055-7.

Tian, W., 2005, Burial history of the Kongquehe region in Tarim Basin, Jinlin University 73 p.

Visser, W., 1982, Maximum diagenetic temperature in a petroleum source-rock from Venezuela by fluid inclusion geothermometry: Chemical Geology, v. 37, p. 95-101, Doi. 10.1016/0009-2541(82)90069-9.

Wei, G., C. Jia, H. Song, Y. Shi, H. Lu, and Y. Li, 2000, Ordovician Structural - Depositional Model and Prediction for Profitable Crack Reservoir of Carbonate Rock in Tazhong Area, Tarim: Acta Sedimentologica Sinica, v. 18, p. 408-413, Doi. 10.14027/j .cnki .cjxb.2000.03.014.

Wenger, L. M., and G. H. Isaksen, 2002, Control of hydrocarbon seepage intensity on level of biodegradation in sea bottom sediments: Organic Geochemistry, v. 33, p. 1277-1292, Doi. 10.1016/S0146-6380(02)00116-X.

Wu, L., Y. Liao, Y. Fang, and A. Geng, 2012, The study on the source of the oil seeps and bitumens in the Tianjingshan structure of the northern Longmen Mountain structure of Sichuan Basin, China: Marine and Petroleum Geology, v. 37, p. 147-161, Doi. 10.1016/j.marpetgeo.2012.05.011.

Xiao, H., J. Zhao, H. Yang, Z. Cai, Y. Zhu, L. Huang, and N. Zhang, 2012, Fluid Inclusion and Micro-FTIR Evidence for Hydrocarbon Charging Fluid Evolution of the Ordovician Reservoir of Halahatang Depression, the Tarim Basin: Earth Science-Journal of China University of Geosciences, v. 37, p. 163-173, Doi. 10.3799/dqkx.2012.S1.016.

Xiao, H., J. Zhao, Y. Zhu, and Y. Li, 2013, Geochemical Tracking on Hydrocarbon Accumulation Periods of Ordovician in Hanilcatam Sag, Tarim Basin: Xinjiang Petroleum Geology, v. 34, p. 465-468.

Xiao, X., and M. Tang, 2003, The Tarim Basin becoming the biggest onshore natural gas production area in China: Natural Gas Geoscience v. 14, p. 35-38.

873 Xiao, Z., M. Li, S. Huang, T. Wang, B. Zhang, R. Fang, K. Zhang, Z. Ni, Q. Zhao, and D. Wang, 2016, Source,
874 oil charging history and filling pathways of the Ordovician carbonate reservoir in the
875 Halahatang Oilfield, Tarim Basin, NW China: Marine and Petroleum Geology, v. 73, p. 59-71,
876 Doi. 10.1016/j.marpetgeo.2016.02.026.
877 Xu, G., C. Lin, Y. Liu, and Q. Sun, 2016, Evolution of Palaeo Uplift and Its Controlling on Sedimentation
878 of Kapushaliang Group of Early Cretaceous in Western Tabei Uplift: Earth Science, v. 41, p.
879 619-632, Doi. 10.3799/dqkx.2016.051.
880 Xu, X., Q. Zhou, and L. Zhang, 2004, Oil and gas reserves and their distribution in Tarim Basin: Oil &
881 Gas Geology, v. 25, p. 300-303.
882 Yang, C., Z. Wang, B. P. Hollebone, C. E. Brown, and M. Landriault, 2009, Characteristics of bicyclic
883 sesquiterpanes in crude oils and petroleum products: Journal of Chromatography A, v. 1216,
884 p. 4475-4484, Doi. 10.1016/j.chroma.2009.03.024.
885 Zhang, G., W. Zhao, H. Wang, H. Li, and L. Liu, 2007a, Multicycle tectonic evolution and composite
886 petroleum systems in the Tarim Basin: Oil & Gas Geology, v. 28, p. 653-663.
887 Zhang, P., S. Zhang, and Y. He, 1990, Issues on oil classification Oil & Gas Storge and Transportation, v.
888 9, p. 74-77.
889 Zhang, S., and H. Huang, 2005, Geochemistry of Palaeozoic marine petroleum from the Tarim Basin,
890 NW China: Part 1. Oil family classification: Organic Geochemistry, v. 36, p. 1204-1214, Doi.
891 10.1016/j.orggeochem.2005.01.013.
892 Zhang, W., S. Zhu, S. He, and Y. Wang, 2015, Screening of oil sources by using comprehensive two-
893 dimensional gas chromatography/time-of-flight mass spectrometry and multivariate
894 statistical analysis: Journal of Chromatography A, v. 1380, p. 162-170, Doi.
895 10.1016/j.chroma.2014.12.068.
896 Zhang, X., Y. Duan, J. He, B. Wu, and L. Xu, 2011, Geochemical Characteristics of Crude Oil in Lower
897 Part of Yanchang Formation and Correlation of Oil Source in Huaqing Area of Ordos Basin:
898 Natural Gas Geoscience v. 22, p. 866-873.
899 Zhang, Y., Z. Horst, K. Liu, and X. Luo, 2007b, K-Ar isotopic dating of authigenic illite and its
900 application to the investigation of hydrocarbon accumulation history of the Silurian
901 bitumious sandstone reservoirs in the Tazhong uplift, Tarim basin: Oil & Gas Geology, v. 28, p.
902 166-174.
903 Zhang, Y., Z. Horst, A. Todd, K. Liu, and X. Luo, 2004, K-Ar dating of authigenic illite and its
904 applications to study of oil-gas charging histories of typical sandstone reservoirs, Tarim
905 Basin, Northwest China: Earth Science Frontiers v. 4, p. 637-648.
906 Zhang, Y., and X. Luo, 2011, K-Ar dating of authigenic illites and hydrocarbon accumulation history of
907 the Silurian bitumious sandstons reservoirs in Yingmai area, Tarim Basin: Petroleum
908 Exploration and Development, v. 38, p. 203-210.
909 Zhao, J., Q. Li, Q. Wang, W. Pang, B. Shi, and J. Luo, 2004, On the formation and distribution of mid-
910 large oil and gas fields in the Tarim Basin: Journal of Northwest University (Nature Science
911 Edition), v. 34, p. 212-217, Doi. 10.16152/j .cnki .xdxbzr.2004.02.022.
912 Zhu, G., H. Yang, Y. Zhu, L. Gu, Y. Lu, J. Su, B. Zhang, and Q. Fan, 2011, Study on petroleum geoligical
913 characteristics and accumulation of carbon reservoirs in Hanilcatam area, Tarim Basin: Acta
914 Petrologica Sinica, v. 27, p. 827-844.
915 Zhu, G., S. Zhang, K. Liu, H. Yang, B. Zhang, J. Su, and Y. Zhang, 2013a, A well-preserved 250 million-
916 year-old oil accumulation in the Tarim Basin, western China: Implications for hydrocarbon
917 exploration in old and deep basins: Marine and Petroleum Geology, v. 43, p. 478-488, Doi.
918 10.1016/j.marpetgeo.2012.12.001.
919 Zhu, G., S. Zhang, J. Su, H. Huang, H. Yang, L. Gu, B. Zhang, and Y. Zhu, 2012, The occurrence of ultra-
920 deep heavy oils in the Tabei Uplift of the Tarim Basin, NW China: Organic Geochemistry, v. 52,
921 p. 88-102, Doi. 10.1016/j.orggeochem.2012.08.012.
922 Zhu, G., S. Zhang, J. Su, S. Meng, H. Yang, J. Hu, and Y. Zhu, 2013b, Secondary accumulation of
923 hydrocarbons in Carboniferous reservoirs in the northern Tarim Basin, China: Journal of
924 Petroleum Science and Engineering, v. 102, p. 10-26, Doi. 10.1016/j.petrol.2013.01.005.
925 Zhu, G., S. Zhang, J. Su, B. Zhang, H. Yang, Y. Zhu, and L. Gu, 2013c, Alteration and multi-stage
926 accumulation of oil and gas in the Ordovician of the Tabei uplift, Tarim Basin, NW China:
927 implications for genetic origin of the diverse hydrocarbons: Marine and Petroleum Geology, v.

46, p. 234-250, Doi. 10.1016/j.marpetgeo.2013.06.007.
Zumberge, J. E., 1987, Prediction of source rock characteristics based on terpane biomarkers in crude oils: A multivariate statistical approach: Geochimica et Cosmochimica Acta, v. 51, p. 1625-1637, Doi. 10.1016/0016-7037(87)90343-7.

Author's vita

Xiang Ge

Key Laboratory of Tectonics and Petroleum Resources (China University of Geosciences), Ministry of Education, Wuhan, 430074, China; 388 Lumo Road, Hongshan District, Wuhan City, Hubei Province, China.

xiangge89@126.com

Xiang Ge is an Associate Professor at the China University of Geoscience (Wuhan) (CUG). He received his B.Sc., M.Sc. and Ph.D from China University of Geoscience (Wuhan). As an joint Ph.D student of CUG and Durham University, his research is focusing on the petroleum geology of the Sichuan and Tarim Basin applying hydrocarbon Re-Os isotope, organic geochemistry, structural and tectonic analyses.

Chuanbo Shen (*Corresponding author)

Key Laboratory of Tectonics and Petroleum Resources (China University of Geosciences), Ministry of Education, Wuhan, 430074, China; 388 Lumo Road, Hongshan District, Wuhan City, Hubei Province, China.

cugshen@126.com

Chuanbo Shen (Corresponding author) is currently a professor in the Faculty of Earth Resources at the China University of Geosciences (Wuhan). He received his B.Sc., M.Sc., and Ph.D. from China University of Geoscience (Wuhan). He also completed postdoctoral research in Technische Universität Bergakademie Freiberg, Germany. His present research interests are low-temperature thermochronology, tectonic-thermal

evolution and hydrocarbon geochronology.

David Selby

Department of Earth Sciences, Durham University, Durham, DH1 3LE, UK

david.selby@durham.ac.uk

David Selby is a Professor of Earth Sciences at Durham University, UK. He received a bachelor's degree in geology from Southampton University, UK and Ph.D. degree from the University of Alberta, Canada. He also carried out his postdoctoral research at the University of Alberta. His research focuses on the Earth Science disciplines of economic geology, petroleum geoscience and paleoclimate / oceanography, principally through the application and development of the novel, state-of-the-art, rhenium-osmium radio isotope methodology.

Martin Feely

Earth and Ocean Sciences, School of Natural Sciences, National University of Ireland, Galway, Ireland

martin.feely@nuigalway.ie

Martin Feely, BSc., MSc., PhD is an emeritus Professor of Earth and Ocean Sciences in the School of Natural Sciences, National University of Ireland, Galway. He is Adjunct Professor of Geological and Environmental Sciences at James Madison University (JMU), Virginia, USA. He has authored/co-authored over 200 scientific articles and papers. His research has focused on fluid inclusion studies, methods and applications for the global mineral and oil research and exploration sectors.

Guangyou Zhu

Research Institute of Petroleum Exploration and Development, PetroChina, 20 Xueyuan Road, Haidian District, Beijing 100083, China;

zhuguangyou@petrochina.com.cn

Guangyou Zhu is now a senior expert of geology and geochemistry at the Research Institute of Petroleum Exploration and Development, PetroChina. He received his B.Sc. and Ph.D. degree from the China University of Petroleum (Huadong). His research interests include source rock formation, petroleum accumulation, thermochemical sulfate reduction, and deep oil and gas phase.

Figure captions

Fig. 1. (A) Location of the Tarim Basin, China. (B) Structural unit distribution of the Tarim Basin. (C) Regional map of the Halahatang depression, Yingmaili Uplift, Luntai Uplift, Lunnan Uplift and the Northern Depression (Substantially modified from (Zhu et al., 2012)). Also shown are the sample locations for the Re-Os analysis of this study and the illite K-Ar analysis (Zhang and Luo, 2011; Zhu et al., 2012). The dash line A-A' shows the location of the cross section profile presented in Figure 8.

Fig. 2. Combined Stratigraphic sequences, hydrocarbon system and tectonic events in the north Tarim Basin. Substantially modified after Chang et al., 2013a; Lin et al., 2015 and Zhang and Huang, 2005

Fig. 3. Photomicrographs of (A) an example of a liquid-rich, two-phase (L+V; L>V) aqueous inclusion (~10 microns in longest dimension) in sample Ha9 and (B) an example of a two-phase hydrocarbon bearing fluid inclusion (~10 microns in longest dimension) in sample Ha9. (C, D) examples of hydrocarbon bearing fluid inclusions under

fluorescent light in sample Ha9.

Fig. 4. GC, *m/z* 191 and *m/z* 217 mass chromatogram of the oil samples (Ha9, Ha11, Ha701, XK4-3 and Ha15-2) in Halahatang oilfield, northern Tarim Basin.

Fig. 5. (A). plots of Pristane/nC$_{17}$ and Phytane/nC$_{18}$ alkane ratios for sampled oils. (B) Histogram of the Pr/Ph ratios for sampled oils. (C) Distribution of the tricyclic terpanes (ratios of C$_{23}$TT/C$_{21}$TT, C$_{23}$TT/C$_{24}$TT, C$_{19}$TT/C$_{23}$TT and C$_{24}$TET/C$_{26}$TT) for the samples oils. (D) Histogram of the Ts/Ts+Tm ratio for the sampled oils. (E) Plots of C29ααα20S/(20S+20R)(~0.43) and C29ββ/(ββ+αα) (~0.57) of the sampled oils. (F) Histogram of the C$_{29}$Nor$_{25}$H/C$_{30}$H ratio for the sampled oils.

Fig. 6. (A) A Th frequency distribution histogram of aqueous, coeval (with hydrocarbon-bearing fluid inclusions) aqueous and hydrocarbon-bearing fluid inclusions in sample Ha9. (B) A Th-salinity bivariate plot of aqueous fluid inclusions in sample Ha9. (C) A bivariate plot of Fv (at 20°C) Th for three selected hydrocarbon bearing fluid inclusions from sample Ha9. Seven oil types after (Bourdet et al., 2008) are also plotted for reference indicating that the fluid inclusion hosted oils in sample Ha9 similar in composition to N. America volatile oils (NA = North America).

Fig. 7. (A) A burial history temperature-time plot for the Halahatang oilfield, showing the key time for oil migration and or accumulation. (B) A Th frequency distribution histogram for aqueous fluid inclusions coeval with hydrocarbon-bearing fluid inclusions

in sample Ha 9. (C) A P-T plot of isopleths and isochores for aqueous and hydrocarbon bearing fluid inclusions in Ha9. Isopleths and isochores of the hydrocarbon fluids are determined using PIT modeling (Montel, 1993; Pironon, 2004), whereas isopleths and isochores for the aqueous fluids were generated using (Duan and Mao, 2006). The dash-point lines: coeval aqueous fluid inclusions (PI with AI). The dash lines: non-coeval aqueous fluid inclusions (AI). The solid lines: three hydrocarbon bearing fluid inclusions (PI)(plotted in Fig 5C) and are coeval with the aqueous fluid inclusions. Intersections between the coeval isochores yield estimates of true fluid trapping temperatures and pressures. See text for discussion.

Fig. 8. Re-Os isochron plot of all oil samples Ha9, Ha9rpt, Ha11, Ha701, XK4-3. Data-point ellipses shown at the 2-sigma level absolute uncertainty. The Re-Os data for all samples, except Ha15-2 and Ha15-2rpt, yield a Re-Os date of 285 ± 48 Ma, with an initial $^{187}Os/^{188}Os$ of 1.08 ± 0.20 (MSWB = 6.1). Ha9rpt and Ha15-2rpt are repeated analysis of samples Ha9 and Ha15-2.

Fig. 9. Petroleum evolution model for the Halahatang oilfield, northern Tarim Basin. (A) Halahatang depression during the Late Silurian. (B). Oil generation during the Early Permian. (C) Oil migration/accumulation process during the Late Permian to Early Triassic. (D) Present day configuration of the Halahatang oilfield after continuous sedimentation since the Late Triassic. See text for discussion.

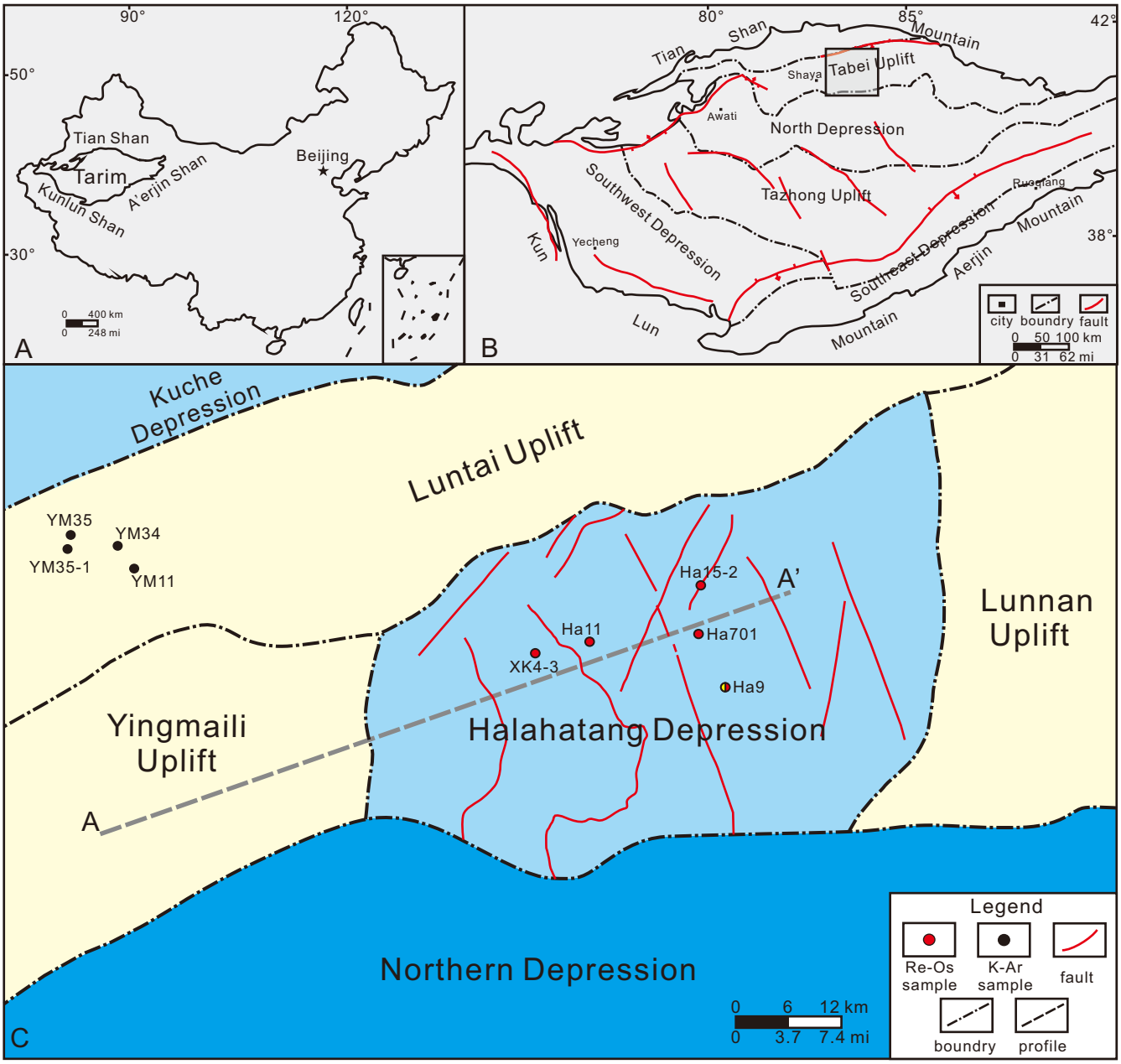
90°
120°
50°
30°
Tian Shan
Tarim
Kunlun Shan
A'erjin Shan
Beijing
0 400 km
0 248 mi
A
80°
85°
42°
38°
Tian Shan Mountain
Tabei Uplift
Shaya
Awati
North Depression
Southwest Depression
Tazhong Uplift
Southeast Depression
Ruoqiang
Kun Lun Mountain
Yecheng
Aerjin Mountain
city boundry fault
0 50 100 km
0 31 62 mi
B
Kuche Depression
Luntai Uplift
YM35
YM34
YM35-1
YM11
Ha15-2
A'
Ha11
Ha701
XK4-3
Ha9
Lunnan Uplift
Yingmaili Uplift
Halahatang Depression
A
Northern Depression
Legend
Re-Os sample
K-Ar sample
fault
boundry
profile
0 6 12 km
0 3.7 7.4 mi
C

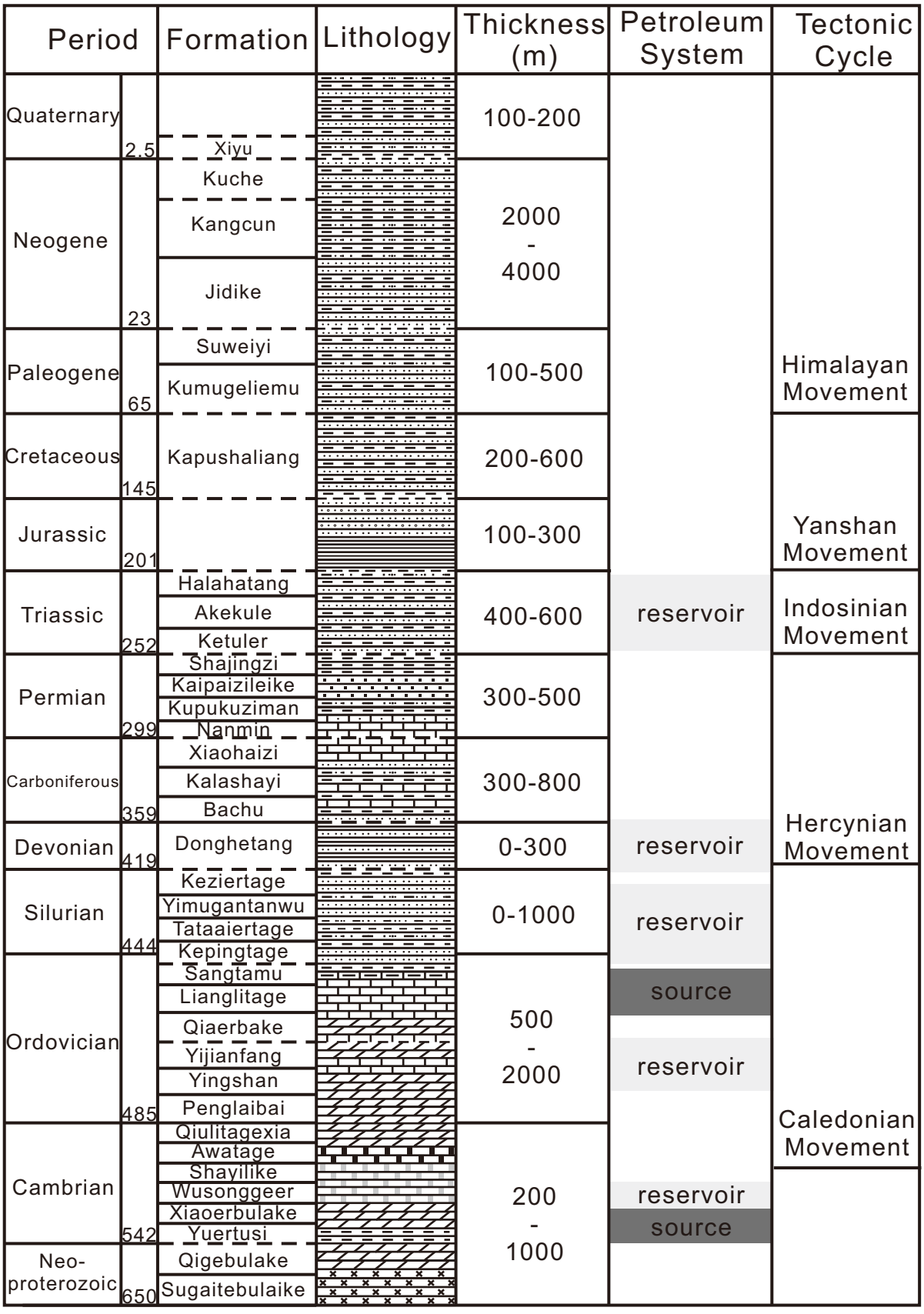
Period
Formation
Lithology
Thickness (m)
Petroleum System
Tectonic Cycle
Quaternary
2.5
Xiyu
100-200
Neogene
23
Kuche
Kangcun
Jidike
2000 - 4000
Paleogene
65
Suweiyi
Kumugeliemu
100-500
Himalayan Movement
Cretaceous
145
Kapushaliang
200-600
Jurassic
201
100-300
Yanshan Movement
Triassic
252
Halahatang
Akekule
Ketuler
400-600
reservoir
Indosinian Movement
Permian
299
Shajingzi
Kaipaizileike
Kupukuziman
Nanmin
300-500
Carboniferous
359
Xiaohaizi
Kalashayi
Bachu
300-800
Devonian
419
Donghetang
0-300
reservoir
Hercynian Movement
Silurian
444
Keziertage
Yimugantanwu
Tataaiertage
Kepingtage
0-1000
reservoir
Ordovician
485
Sangtamu
Lianglitage
Qiaerbake
Yijianfang
Yingshan
Penglaibai
500 - 2000
source
reservoir
Caledonian Movement
Cambrian
542
Qiulitagexia
Awatage
Shayilike
Wusonggeer
Xiaoerbulake
Yuertusi
200 - 1000
reservoir
source
Neo-proterozoic
650
Qigebulake
Sugaitebulaike

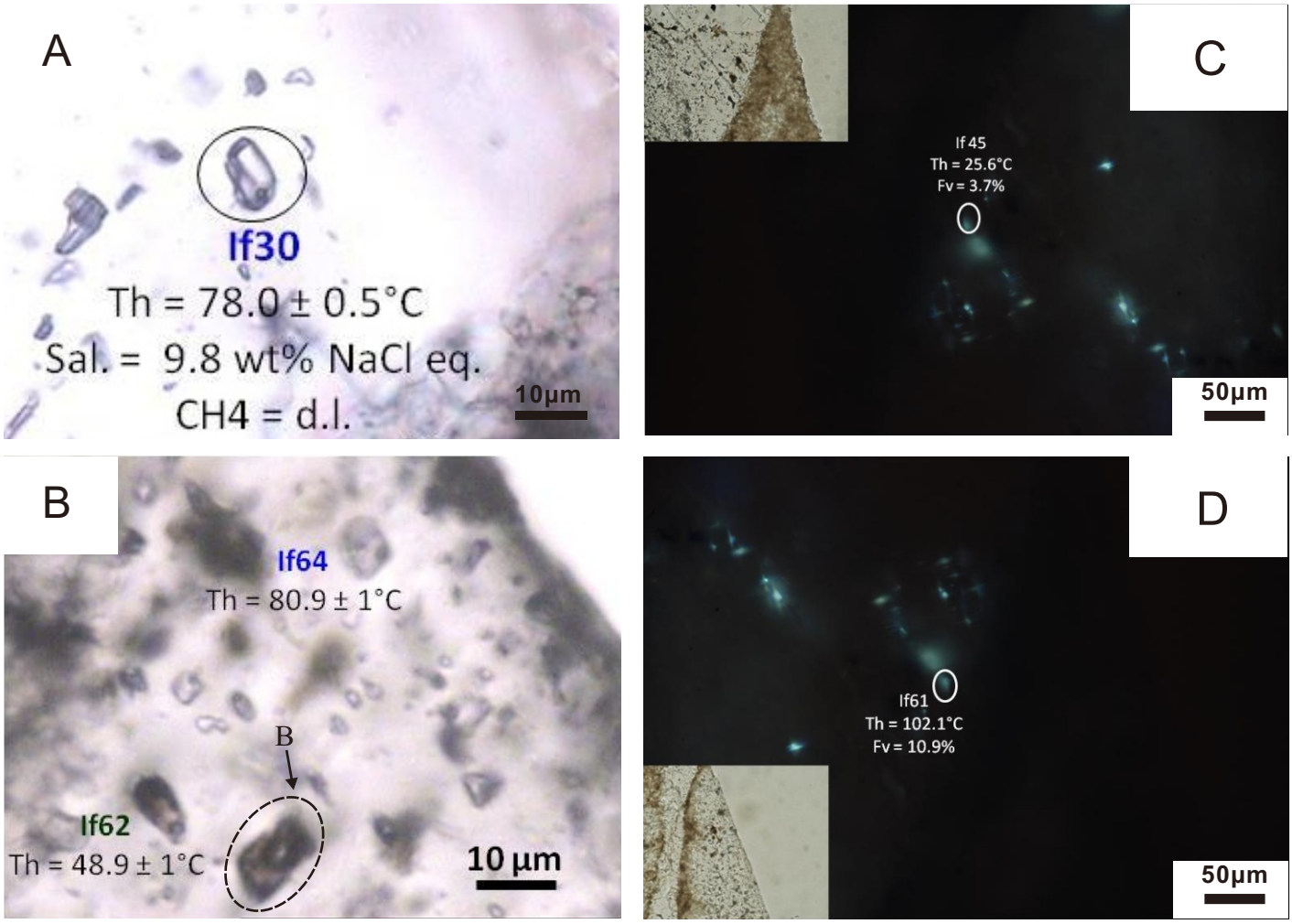
A
If30
Th = 78.0 ± 0.5°C
Sal. = 9.8 wt% NaCl eq.
CH4 = d.l.
10µm
C
If 45
Th = 25.6°C
Fv = 3.7%
50µm
B
If64
Th = 80.9 ± 1°C
B
If62
Th = 48.9 ± 1°C
10 µm
D
If61
Th = 102.1°C
Fv = 10.9%
50µm

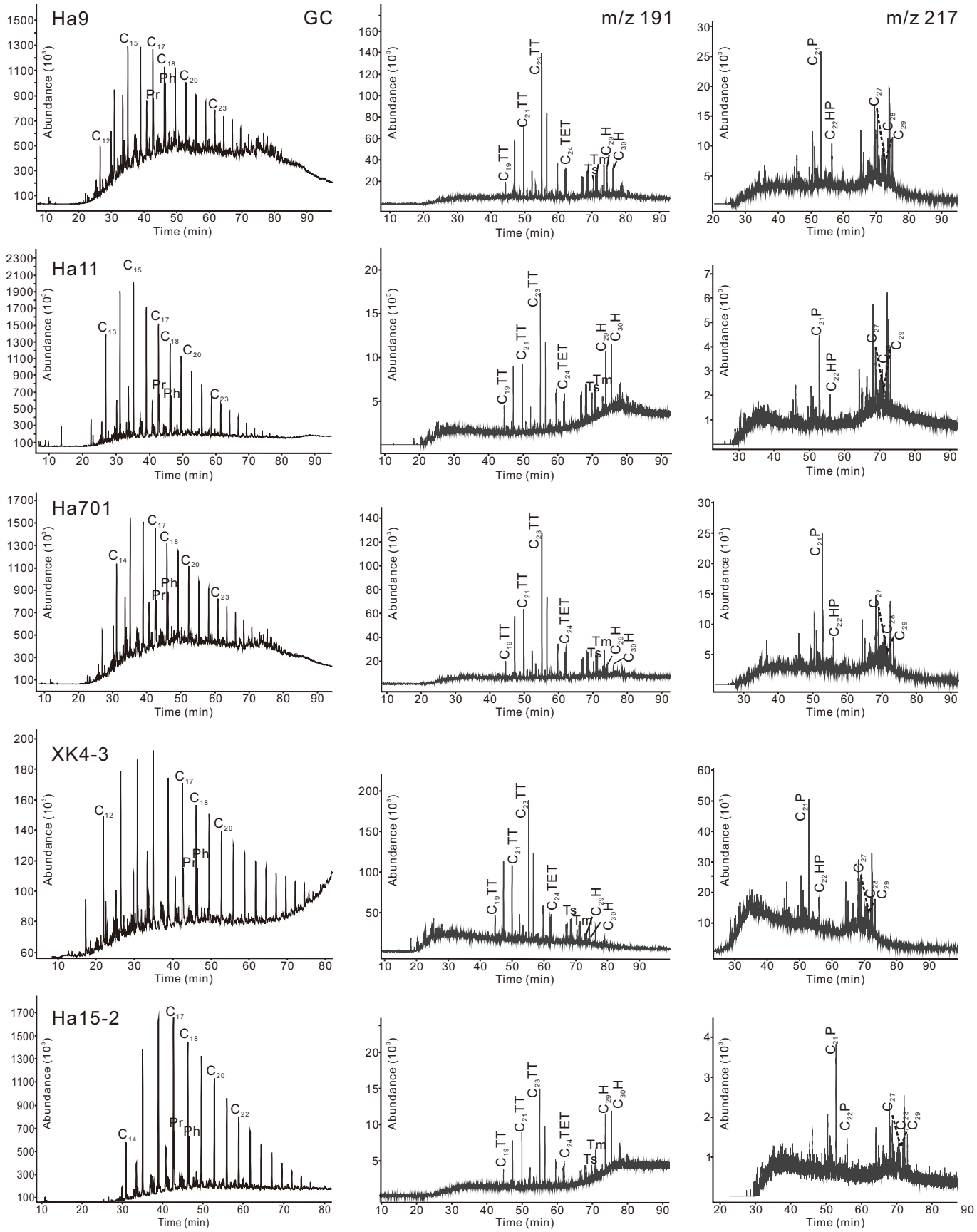
Ha9
GC
m/z 191
m/z 217
Ha11
Ha701
XK4-3
Ha15-2
Abundance (10³)
Time (min)
C12
C13
C14
C15
C17
C18
C19 TT
C20
C21 TT
C22
C22HP
C23
C23 TT
C24 TET
C27
C28
C29
C29H
C30H
Pr
Ph
Tm
Ts

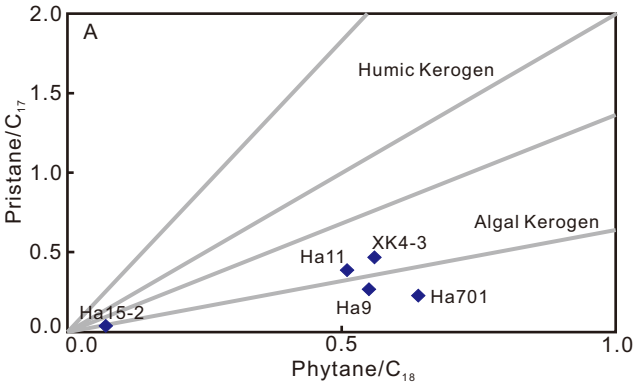
A
Humic Kerogen
Algal Kerogen
Ha11
XK4-3
Ha9
Ha701
Ha15-2
Pristane/C17
Phytane/C18
2.0
1.5
1.0
0.5
0.0
0.0
0.5
1.0

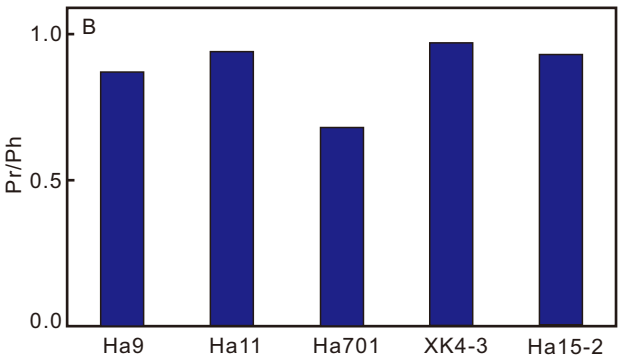
B
Pr/Ph
1.0
0.5
0.0
Ha9
Ha11
Ha701
XK4-3
Ha15-2

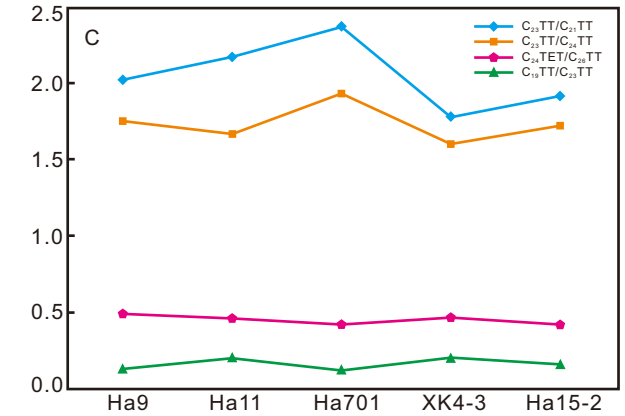
C
C23TT/C21TT
C23TT/C24TT
C24TET/C26TT
C19TT/C23TT
2.5
2.0
1.5
1.0
0.5
0.0
Ha9
Ha11
Ha701
XK4-3
Ha15-2

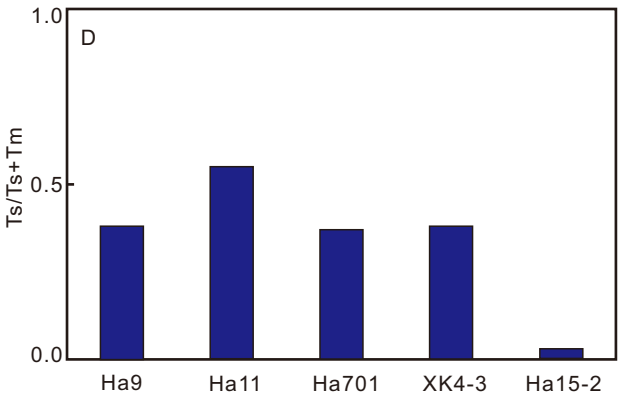
D
Ts/Ts+Tm
1.0
0.5
0.0
Ha9
Ha11
Ha701
XK4-3
Ha15-2

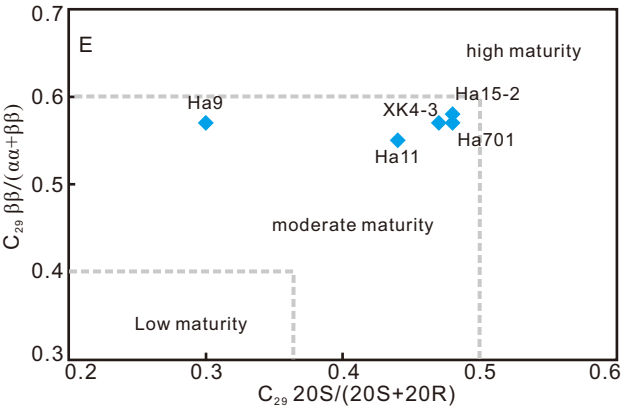
E
high maturity
moderate maturity
Low maturity
Ha9
Ha15-2
XK4-3
Ha701
Ha11
C29 ββ/(αα+ββ)
C29 20S/(20S+20R)
0.7
0.6
0.5
0.4
0.3
0.2
0.3
0.4
0.5
0.6

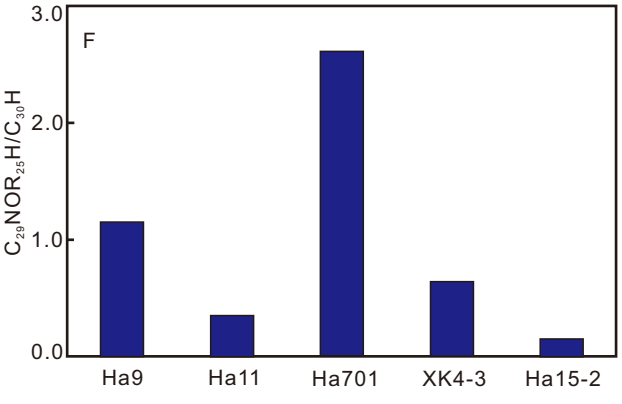
F
C28NOR25H/C30H
3.0
2.0
1.0
0.0
Ha9
Ha11
Ha701
XK4-3
Ha15-2

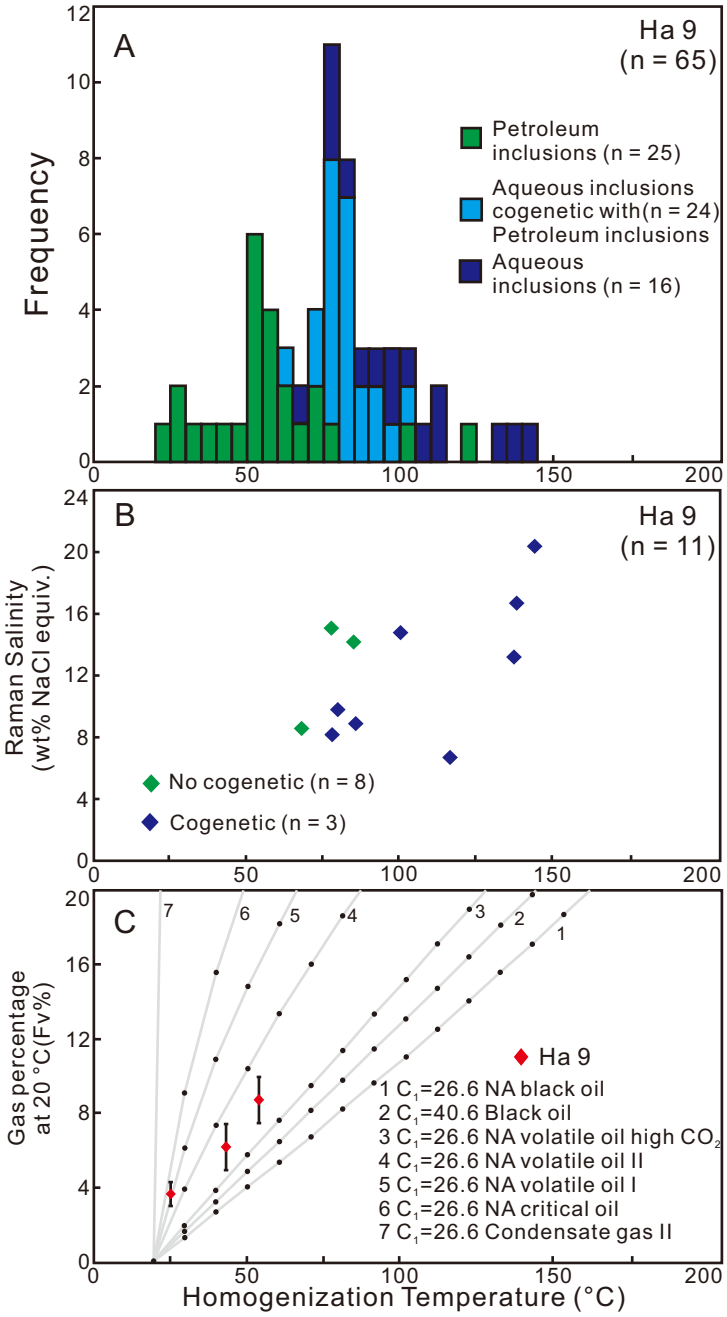
A
Ha 9
(n = 65)
Petroleum inclusions (n = 25)
Aqueous inclusions cogenetic with(n = 24) Petroleum inclusions
Aqueous inclusions (n = 16)
Frequency
B
Ha 9
(n = 11)
No cogenetic (n = 8)
Cogenetic (n = 3)
Raman Salinity (wt% NaCl equiv.)
C
Ha 9
1 C1=26.6 NA black oil
2 C1=40.6 Black oil
3 C1=26.6 NA volatile oil high CO2
4 C1=26.6 NA volatile oil II
5 C1=26.6 NA volatile oil I
6 C1=26.6 NA critical oil
7 C1=26.6 Condensate gas II
Gas percentage at 20 °C(Fv%)
Homogenization Temperature (°C)

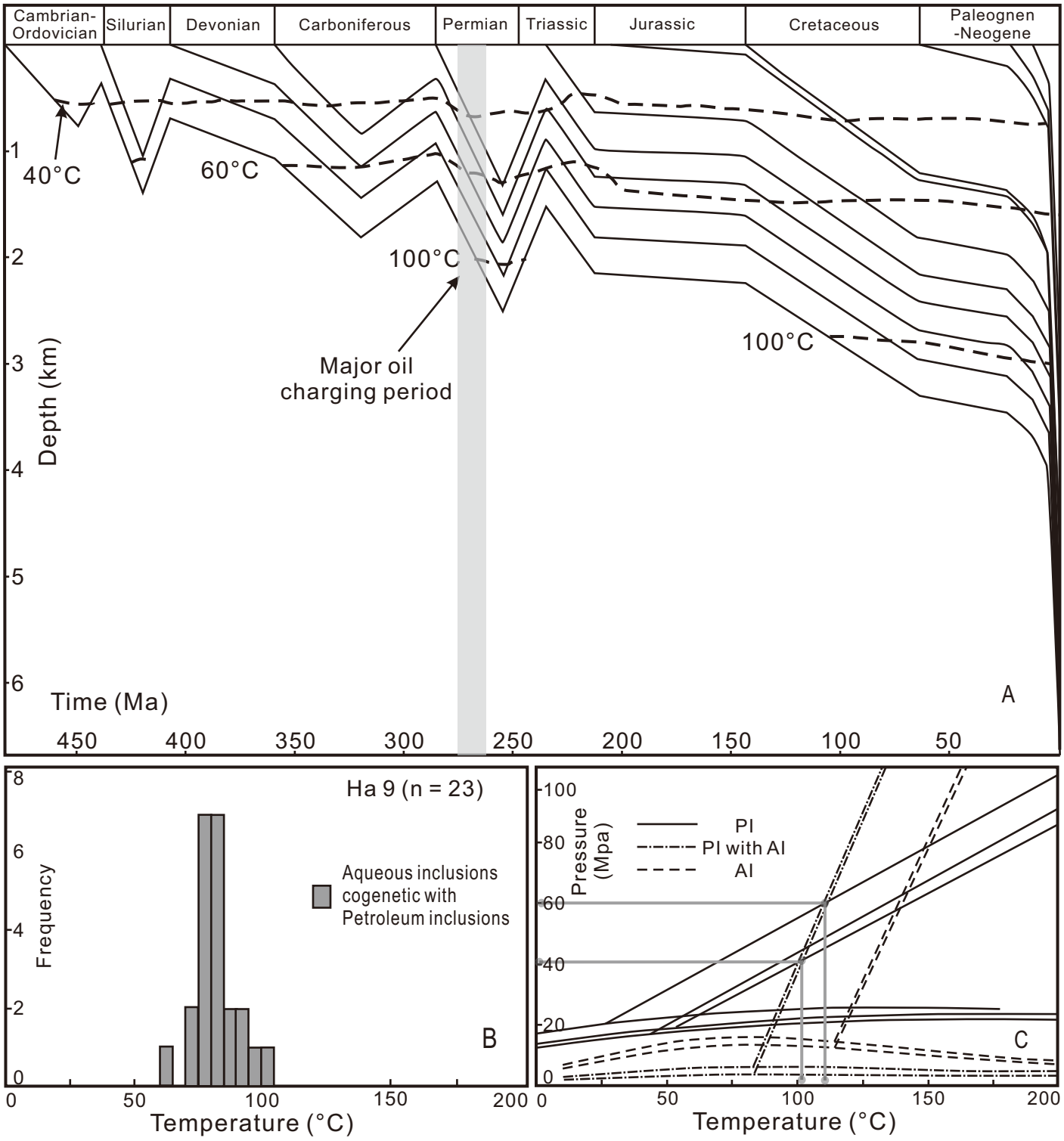
Cambrian-
Ordovician
Silurian
Devonian
Carboniferous
Permian
Triassic
Jurassic
Cretaceous
Paleognen
-Neogene
40°C
60°C
100°C
100°C
Major oil
charging period
Depth (km)
Time (Ma)
A
Ha 9 (n = 23)
Aqueous inclusions
cogenetic with
Petroleum inclusions
Frequency
Temperature (°C)
B
Pressure
(Mpa)
PI
PI with AI
AI
Temperature (°C)
C

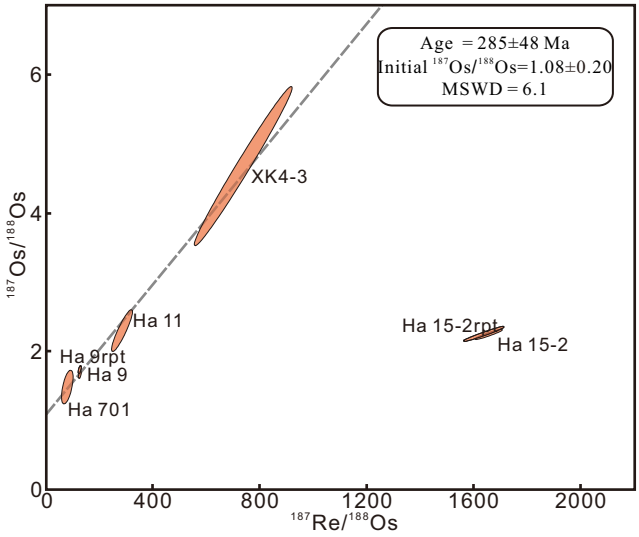
Age = 285±48 Ma
Initial 187Os/188Os=1.08±0.20
MSWD = 6.1
XK4-3
Ha 11
Ha 9rpt
Ha 9
Ha 701
Ha 15-2rpt
Ha 15-2
187Os/188Os
187Re/188Os
0
2
4
6
0
400
800
1200
1600
2000

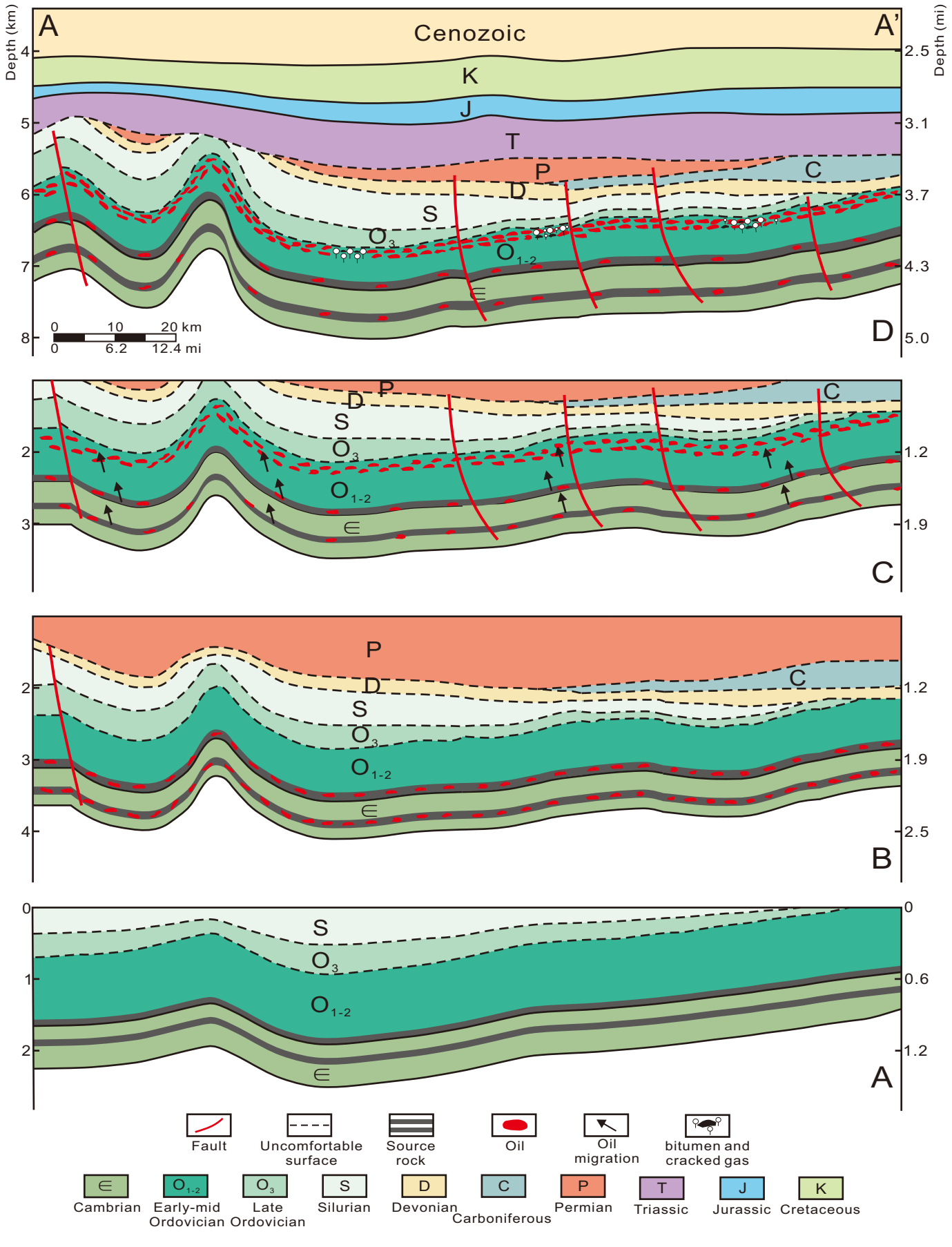
A
A'
Cenozoic
K
J
T
P
D
S
C
O_3
O_{1-2}
∈
Depth (km)
Depth (mi)
0 10 20 km
0 6.2 12.4 mi
D
C
B
A
Fault
Uncomfortable surface
Source rock
Oil
Oil migration
bitumen and cracked gas
Cambrian
Early-mid Ordovician
Late Ordovician
Silurian
Devonian
Carboniferous
Permian
Triassic
Jurassic
Cretaceous

Table 1. Physical properties, sulfur content and component of the oil from the halahatang oilfield.

Well name	Depth (m)	Formation Name	Density (g/cm3)		Viscosity (mPa·s, 50 ºC)	API vaule	Wax (%)	Sulfur (%)	Saturate (%)	Aromatic (%)	Resin (%)	Asphaltene (%)
			20 ºC	50 ºC								
Ha 9	6598-6710	Ordovician Yijianfang	0.879	0.859	6.92	29.48	3.80	0.84	57.33	10.00	6.67	23.33
Ha 11	6658-6748	Ordovicia Yijianfang	0.833	0.812	2.62	38.37	6.10	0.50	64.67	14.33	3.67	14.33
Ha 15-2	6559-6598	Ordovician Yijianfang	0.844	0.822	3.15	36.15	8.60	0.63	56.00	18.00	4.33	18.67
Ha 701	6557-6618	Ordovician Yijianfang	1.011	0.992	342.3	8.46	/	0.67	46.92	13.36	3.42	33.56
XK4-3	6834-6850	Ordovician Yijianfang	0.88	0.86	7.96	29.30	5.90	0.59	55.49	26.55	5.24	3.56

/: Not measured

Table 2. The biomarker parameters of the oil samples from Halahatang oilfield.

Sample name	Pr/nC$_{17}$	Ph/nC$_{18}$	Pr/Ph	C$_{23}$TT/C$_{21}$TT	C$_{23}$TT/C$_{24}$TT	C$_{19}$TT/C$_{23}$TT	C$_{24}$TET/C$_{26}$TT	Ts/(Ts+Tm)	GAM/C$_{30}$H
Ha9	0.27	0.55	0.87	2.02	1.75	0.13	0.49	0.38	0.19
Ha11	0.39	0.51	0.94	2.17	1.67	0.20	0.46	0.55	0.12
Ha701	0.23	0.64	0.68	2.37	1.93	0.12	0.42	0.37	0.15
XK4-3	0.47	0.56	0.97	1.78	1.60	0.20	0.47	0.38	0.05
Ha15-2	0.04	0.07	0.93	1.91	1.72	0.16	0.42	0.03	0.07
	C$_{30}$DH/ C$_{30}$H	**C$_{29}$NOR$_{25}$H/ C$_{30}$H**	**C$_{21}$P/C$_{22}$HP**	**C$_{27}$R (%)**	**C$_{28}$R (%)**	**C$_{29}$R (%)**	**C$_{29}$ ααα20S/(20S+20R)**	**C$_{29}$ ββ/(ββ+αα)**	
Ha9	0.10	1.15	3.12	56.69	7.56	35.75	0.30	0.57	
Ha11	0.03	0.35	2.98	37.40	20.07	42.53	0.44	0.55	
Ha701	0.13	2.61	4.20	65.37	7.02	27.60	0.48	0.57	
XK4-3	0.10	0.64	5.69	49.64	15.96	34.39	0.47	0.57	
Ha15-2	0.10	0.15	4.15	42.20	22.70	35.11	0.48	0.58	

Table 3. Summary of petrographic observations, microthermometry, Laser Raman Microspectroscopy and CSLM results of aqueous and oil-bearing inclusions for sample Ha9.

Sample Name	Inclusion No.	FI types	types	Th (ºC)	Error (ºC)	Raman Salinity wt% (NaCl aq.)	Raman Salinity (molal)	CH_4 (molal)	Bulk volume (μm^3)	Bubble volume (μm^3)	Fv at 20ºC (%)	Relative error %
Ha 9-1A	42	2-phase L-V oil	Calcite cement	52.8	2							
Ha 9-1A	43	2-phase L-V oil	Calcite cement	52.6	1							
Ha 9-1A	44	2-phase L-V aqueous	Calcite cement	98.1	0.2	14.6	3.02	0.1				
Ha 9-1A	45	2-phase L-V oil	Calcite cement	25.6	0.5				94.7	3.5	3.7	17
Ha 9-1B	45b	2-phase L-V oil	Calcite cement	n.m					32.6	1.8	5.1	49
Ha 9-1B	46	2-phase L-V aqueous	Calcite cement	85.8	2							
Ha 9-1B	47	2-phase L-V oil	Calcite cement	25.1	0.3							
Ha 9-1B	48	2-phase L-V aqueous	Calcite cement	71.7	0.3							
Ha 9-1B	49	2-phase L-V oil	Calcite cement	57.2	0.2							
Ha 9-1B	50	2-phase L-V aqueous	Calcite cement	86.7	2							
Ha 9-1B	68	2-phase L-V aqueous	Calcite cement	83.2	0.2	14.2	2.88	0.017-0.026				
Ha 9-1B	69	1-phase L aqueous	Calcite cement			18.6	4.04					
Ha 9-1C	51	2-phase L-V oil	Calcite cement	54.2	0.2							
Ha 9-1C	52	2-phase L-V oil	Calcite cement	24.6	0.3							
Ha 9-1C	53	2-phase L-V oil	Calcite cement	29.2	0.3							
Ha 9-1C	54	2-phase L-V oil	Calcite cement	37	0.2							
Ha 9-1C	55	2-phase L-V aqueous	Calcite cement	83.8	1							
Ha 9-1C	56	2-phase L-V aqueous	Calcite cement	91.6	2							
Ha 9-1C	57	2-phase L-V aqueous	Calcite cement	107.1	2							
Ha 9-1C	58	2-phase L-V aqueous	Calcite cement	77	1							
Ha 9-1C	59	2-phase L-V aqueous	Calcite cement	76.1	1	15.1	3.1	n.m.				
Ha 9-1C	60	2-phase L-V aqueous	Calcite cement	83.3	0.5							
Ha 9-1D	61b	2-phase L-V oil	Calcitized bioclast	122	2							
Ha 9-1D	62	2-phase L-V oil	Calcitized bioclast	48.9	1							
Ha 9-1D	63	2-phase L-V aqueous	Calcitized bioclast	79.5	0.5							
Ha 9-1D	64	2-phase L-V aqueous	Calcitized bioclast	80.9	1							
Ha 9-1D	65	2-phase L-V aqueous	Calcitized bioclast	82.9	1							
Ha 9-1D	67	2-phase L-V aqueous	Calcitized bioclast	79.6	1							
Ha 9-2A	1	2-phase L-V aqueous	Calcitized bioclast	90.6	0.5							
Ha 9-2A	2	2-phase L-V aqueous	Calcite cement	76.1	0.5							
Ha 9-2A	3	2-phase L-V aqueous	Calcite cement	102.3	1							
Ha 9-2A	7	2-phase L-V aqueous	Calcite cement	75.4	1							
Ha 9-2A	8	2-phase L-V aqusous	Calcite cement	74	0.3							
Ha 9-4A	10	2-phase L-	Calcite	77.3	0.3							

		V aqueous	cement									
Ha 9-4A	11	2-phase L-V aqueous	Calcite cement	75.1	1							
Ha 9-4A'	12	2-phase L-V oil	Calcite cement	59.1	0.5							
Ha 9-4A'	13	2-phase L-V oil	Calcite cement	58.1	2							
Ha 9-4B	15	3-phase L-V oil	Calcitized bioclast	50.8	1							
Ha 9-4C	16	2-phase L-V oil	Calcitized bioclast	60	1							
Ha 9-4C	17	2-phase L-V oil	Calcitized bioclast	30.9	1							
Ha 9-4C	18	2-phase L-V oil	Calcitized bioclast	79.9	1							
Ha 9-4D	20	2-phase L-V aqueous	Calcite cement	66.4	0.5	8.6	1.63	n.m.				
Ha 9-4D	21	2-phase L-V aqueous	Calcite cement	66.3	2	9.5	1.82	d.l.				
Ha 9-4D	21b	2-phase L-V aqueous	Calcite cement	117	1	6.7	1.24	0.067-0.075				
Ha 9-4D	21c	2-phase L-V aqueous	Calcite cement	134.3	2	13.2	2.63	n.m.				
Ha 9-4D	22	2-phase L-V oil	Calcite cement	53.5	0.3				29.4	2.6	8.7	14
Ha 9-4E	23	2-phase L-V oil	Calcitized bioclast	68.1	0.5							
Ha 9-4E	24	3-phase L-V oil	Calcitized bioclast	63.4	2							
Ha 9-4E	25	2-phase L-V oil	Calcitized bioclast	43.1	1				84.4	5.6	6.2	20
Ha 9-4E	26	2-phase L-V oil	Calcitized bioclast	51.8	2							
Ha 9-4E	26b	2-phase L-V oil	Calcitized bioclast	n.m.					21.8	1.6	6.7	19
Ha 9-5A	27	2-phase L-V aqueous	Calcitized bioclast	61.2	0.3							
Ha 9-5A	28	2-phase L-V aqueous	Calcitized bioclast	99.3	2							
Ha 9-5A	70	2-phase L-V aqueous	Calcitized bioclast	135.2	1	16.7	3.51	d.l.				
Ha 9-5A	71	2-phase L-V aqueous	Calcitized bioclast	141.1	1	20.4	4	d.l.				
Ha 9-5B	30	2-phase L-V aqueous	Calcite cement	78	0.5	9.8	1.87	d.l.				
Ha 9-5B	31	2-phase L-V aqueous	Calcite cement	76.4	0.3	8.2	1.55	d.l.				
Ha 9-5B	32	2-phase L-V aqueous	Calcite cement	111	1							
Ha 9-5B	33	2-phase L-V aqueous	Calcite cement	95.5	1							
Ha 9-5B	34	2-phase L-V aqueous	Calcite cement	83.8	0.5	8.9	1.69	d.l.				
Ha 9-5B	35	2-phase L-V aqueous	Calcite cement	100.3	1							
Ha 9-5B	35b	2-phase L-V aqueous	Calcite cement	n.m.		9.3	1.77	d.l.				
Ha 9-5C	36	2-phase L-V oil	Calcitized bioclast	72.7	1							
Ha 9-5C	37	2-phase L-V oil	Calcitized bioclast	71.2	1							
Ha 9-7A	38	2-phase L-V oil	Calcitized bioclast	51.4	0.3							
Ha 9-7A	39	2-phase L-V aqueous	Calcitized bioclast	84.5	0.5							
Ha 9-7A	40	2-phase L-V aqueous	Calcitized bioclast	92	1							
Ha 9-7A	41	2-phase L-V aqueous	Calcitized bioclast	84	0.3							

Table 4. Synopsis of the Re-Os isotopic data of asphaltene fractions from oil from the Halahatang oilfield, Tarim basin, China.

Sample	Re (ppb)	±	Os (ppt)	±	^{192}Os (ppt)	±	^{187}Re/^{188}Os	±	^{187}Os/^{188}Os	±	rho	*Osi$_{285Ma}$
Ha 9	0.81	0.01	37.4	0.4	12.9	0.2	125.4	2.8	1.66	0.04	0.723	1.06
Ha 9rpt	1.23	0.02	57.2	0.7	19.5	0.4	125.2	3.2	1.74	0.04	0.732	1.14
Ha11	0.56	0.02	12.1	0.5	3.9	0.4	283.3	30.4	2.30	0.24	0.920	0.95
Ha701	0.07	0.01	4.9	0.3	1.7	0.2	78.7	16.0	1.48	0.19	0.612	1.11
XK4-3	0.85	0.02	8.8	0.6	2.3	0.5	736.8	147.9	4.68	0.93	0.989	1.17
Ha15-2	9.47	0.03	35.2	0.5	11.4	0.3	1655.2	39.7	2.25	0.05	0.970	-5.63
Ha15-2rpt	5.86	0.02	22.0	0.4	7.1	0.3	1636.7	59.9	2.25	0.08	0.983	-5.54

*Osi$_{285Ma}$ = ^{187}Os/^{188}Os measured calculated at the time of oil generation (258 Ma) to yield the initial ^{187}Os/^{188}Os composition.